Received: 7 September 2022 | Revised: 21 May 2023 | Accepted: 21 August 2023

DOI: 10.1002/cac2.12479

CANCER COMMUNICATIONS Open Access

ORIGINAL ARTICLE

JARID2 coordinates with the NuRD complex to facilitate breast tumorigenesis through response to adipocyte-derived leptin

Wei Liu[1,2] | Yi Zeng[1,3] | Xinhui Hao[1] | Xin Wang[4] | Jiaxiang Liu[4] | Tianyang Gao[1] | Mengdi Wang[1] | Jingyao Zhang[2] | Miaomiao Huo[2] | Ting Hu[2] | Tianyu Ma[2] | Die Zhang[2] | Xu Teng[5] | Hefen Yu[5] | Min Zhang[2] | Baowen Yuan[2] | Wei Huang[5] | Yunkai Yang[2] | Yan Wang[1,2]

[1]Key Laboratory of Immune Microenvironment and Disease (Ministry of Education), Department of Biochemistry and Molecular Biology, School of Basic Medical Sciences, Tianjin Medical University, Tianjin, P. R. China

List of abbreviations: JARID2, jumonji and AT-rich interaction domain containing 2; NuRD, nucleosome remodeling and deacetylase; MTA1, metastasis associated 1; PRC1, polycomb repressive complex 1; ES cells, embryonic stem cells; UIM, ubiquitin interaction motif; PRC2, polycomb repressive complex 2; TNBC, triple-negative breast cancer; TSGs, tumor suppressor genes; IHC, immunohistochemistry; TCGA, The Cancer Genome Atlas; GEO, Gene Expression Omnibus; EdU, 5-ethynyl-2-deoxyuridine; CSCs, cancer stem cells; RNA-seq, RNA sequencing; DEGs, differentially expressed genes; FPKM, fragments per kilobase per million mapped fragments; ACTB, actin beta; KEGG, Kyoto Encyclopedia of Genes and Genomes; EMT, epithelial to mesenchymal transition; RT-qPCR, quantitative reverse transcription-polymerase chain reaction; GSEA, Gene Set Enrichment Analysis; shRNA, small hairpin RNA; esiRNA, endoribonuclease-prepared siRNA; hEGF, human recombinant epidermal growth factor; bFGF, basic fibroblast growth factor; FA, fatty acid; TG, triglyceride; SDS-PAGE, sodium dodecyl sulfate-polyacrylamide gel electrophoresis; Nu-PAGE, Nu-polyacrylamide gel electrophoresis; GST, Glutathione S-transferase; SANT, Swi3-Ada2-N-CoR-TFIIIB domain; ChIP-seq, chromatin IP-based deep sequencing; qChIP, quantitative ChIP; PI3K, phosphatidylinositol 3-kinase; JAK2/STAT3, Janus kinase 2 /signal transducer and activator of transcription 3; MAPK/ERK, mitogen-activated protein kinase; NES, normalized enrichment score; cDNAs, complementary DNAs; ATCC, American Type Culture Collection; FBS, fetal bovine serum; MEBM, mammary epithelium basal medium; DMEM, Dulbecco's modified Eagle's medium; co-IP, co-immunoprecipitation; PBS, phosphate-buffered saline; IB, immunoblotting; ECAR, extracellular acidification rate; SD, standard deviation; ANOVA, analysis of variance; DMFS, distant metastasis-free survival; RFS, relapse-free survival; OS, overall survival; MFS, metastasis-free survival; NF-κB, nuclear factor kappa-light-chain-enhancer of activated B cells; mTORC1, mammalian target of rapamycin complex; RB1, RB transcriptional corepressor 1; BRCA2, BRCA2 DNA repair associated; INPP4B, inositol polyphosphate-4-phosphatase type II B; AEBP2, AE binding protein 2; PHF20L1, PHD finger protein 20 like 1; OCT4, POU class 5 homeobox 1; KLF4, KLF transcription factor 4; c-Myc, MYC proto-oncogene, bHLH transcription factor; SOX2, SRY-box transcription factor 2; NANOG, Nanog homeobox; PPARG, peroxisome proliferator activated receptor gamma; LACTB, lactamase beta; HBP1, HMG-box transcription factor 1; DNAJB4, DnaJ heat shock protein family (Hsp40) member B4; CXADR, CXADR Ig-like cell adhesion molecule; MAMDC2, MAM domain containing 2; HK2, hexokinase 2; PGK1, phosphoglycerate kinase 1; LDHA, lactate dehydrogenase A; ENO1, enolase 1; ENO2, enolase 2; PGAM1, phosphoglycerate mutase 1; SLC2A1, solute carrier family 2 member 1; SLC2A4, solute carrier family 2 member 4; GP1, glucose-6-phosphate isomerase; ALDOA, aldolase, fructose-bisphosphate A; ACLY, ATP citrate lyase; AGPAT1, 1-acylglycerol-3-phosphate O-acyltransferase 1; FADS2, fatty acid desaturase 2; GAPDH, glyceraldehyde-3-phosphate dehydrogenase; GPAM, glycerol-3-phosphate acyltransferase, mitochondrial; INSIG1, insulin induced gene 1; LPIN1, lipin 1; PLIN3, perilipin 3; SCD, stearoyl-CoA desaturase; SREBF1, sterol regulatory element binding transcription factor 1; SUZ12, SUZ12 polycomb repressive complex 2 subunit; EED, embryonic ectoderm development; EZH2, enhancer of zeste 2 polycomb repressive complex 2 subunit; RbAp46/48, RB binding protein 7/4, chromatin remodeling factor; CHD4, chromodomain helicase DNA binding protein 4; HDAC2, histone deacetylase 2; MTA2, metastasis associated 1 family member 2; MBD3, methyl-CpG binding domain protein 3; HDAC1, histone deacetylase 1; GADD45A, growth arrest and DNA damage inducible alpha; SIAH1, siah E3 ubiquitin protein ligase 1; CDKN1A, cyclin dependent kinase inhibitor 1A; FOXK2, forkhead box K2; AKAP12, A-kinase anchoring protein 12; SOCS1, suppressor of cytokine signaling 1; PPARγ, peroxisome proliferator activated receptor gamma; LEPR, leptin receptor; NOTCH1, notch receptor 1; PD1, programmed cell death 1; JAK2, Janus kinase 2; IL6, interleukin 6; MIF, macrophage migration inhibitory factor; TIMP1, TIMP metallopeptidase inhibitor 1; TIMP2, TIMP metallopeptidase inhibitor 2; IGFBP1, insulin like growth factor binding protein 1; SERPINE1, serpin family E member 1.

Wei Liu and Yi Zeng contributed equally to this work.

[2]Key Laboratory of Cancer and Microbiome, State Key Laboratory of Molecular Oncology, National Cancer Center/National Clinical Research Center for Cancer/Cancer Hospital, Chinese Academy of Medical Sciences and Peking Union Medical College, Beijing, P. R. China

[3]Department of Biochemistry and Molecular Biology, School of Basic Medical Science, Southwest Medical University, Luzhou, Sichuan, P. R. China

[4]Department of Breast Surgical Oncology, National Cancer Center/National Clinical Research Center for Cancer/Cancer Hospital, Chinese Academy of Medical Sciences and Peking Union Medical College, Beijing, P. R. China

[5]Beijing Key Laboratory of Cancer Invasion and Metastasis Research, Department of Biochemistry and Molecular Biology, School of Basic Medical Sciences, Capital Medical University, Beijing, P. R. China

Correspondence
Yan Wang and Yunkai Yang, Key Laboratory of Cancer and Microbiome, State Key Laboratory of Molecular Oncology, National Cancer Center/National Clinical Research Center for Cancer/Cancer Hospital, Chinese Academy of Medical Sciences and Peking Union Medical College, Beijing 100021, P. R. China.
Email: yanwang@tmu.edu.cn; yanwang@cicams.ac.cn and ykyang17@fudan.edu.cn

Wei Huang, Beijing Key Laboratory of Cancer Invasion and Metastasis Research, Department of Biochemistry and Molecular Biology, School of Basic Medical Sciences, Capital Medical University, Beijing 100069, P. R. China.
Email: weihuang@ccmu.edu.cn

Funding information
National Natural Science Foundation of China, Grant/Award Numbers: 41931291, 42125707, 82273403, 82203820, 82002993; Major State Basic Research Development Program of China, Grant/Award Number: 2022YFA1103402; Non-profit Central Research Institute Fund of Chinese Academy of Medical Sciences, Grant/Award Numbers: 2019PT310027, 2021-RC310-006; Chinese Academy of Medical Sciences Innovation Fund for Medical Sciences, Grant/Award Number: 2021-I2M-1-018; China Postdoctoral Science Foundation, Grant/Award Number: 2022M710454

Abstract

Background: Proteins containing the Jumonji C (JmjC) domain participated in tumorigenesis and cancer progression. However, the mechanisms underlying this effect are still poorly understood. Our objective was to investigate the role of Jumonji and the AT-rich interaction domain-containing 2 (JARID2) — a JmjC family protein — in breast cancer, as well as its latent association with obesity.

Methods: Immunohistochemistry, The Cancer Genome Atlas, Gene Expression Omnibus, and other databases were used to analyze the expression of JARID2 in breast cancer cells. Growth curve, 5-ethynyl-2-deoxyuridine (EdU), colony formation, and cell invasion experiments were used to detect whether JARID2 affected breast cancer cell proliferation and invasion. Spheroidization-based experiments and xenotumor transplantation in NOD/SCID mice were used to examine the association between JARID2 and breast cancer stemness. RNA-sequencing, Kyoto Encyclopedia of Genes and Genomes, and Gene Set Enrichment Analysis were used to identify the cell processes in which JARID2 participates. Immunoaffinity purification and silver staining mass spectrometry were conducted to search for proteins that might interact with JARID2. The results were further verified using co-immunoprecipitation and glutathione S-transferase (GST) pull-down experiments. Using chromatin immunoprecipitation (ChIP) sequencing, we sought the target genes that JARID2 and metastasis-associated protein 1 (MTA1) jointly regulated; the results were validated by ChIP-PCR, quantitative ChIP (qChIP) and ChIP-reChIP assays. A coculture experiment was used to explore the interactions between breast cancer cells and adipocytes.

Results: In this study, we found that JARID2 was highly expressed in multiple types of cancer including breast cancer. JARID2 promoted glycolysis, lipid metabolism, proliferation, invasion, and stemness of breast cancer cells. Furthermore, JARID2 physically interacted with the nucleosome remodeling and deacetylase (NuRD) complex, transcriptionally repressing a series of tumor suppressor genes such as BRCA2 DNA repair associated (*BRCA2*), RB transcriptional corepressor 1 (*RB1*), and inositol polyphosphate-4-phosphatase type II B (*INPP4B*). Additionally, JARID2 expression was regulated by the obesity-associated adipokine leptin via Janus kinase 2/signal transducer and activator of transcription 3 (JAK2/STAT3) pathway in the breast cancer microenvironment. Analysis of various online databases also indicated that JARID2/MTA1 was associated with a poor prognosis of breast cancer.

Conclusion: Our data indicated that JARID2 promoted breast tumorigenesis and development, confirming JARID2 as a target for cancer treatment.

KEYWORDS
breast tumorigenesis, JARID2, metabolism, the NuRD complex, tumor suppressor genes

1 | BACKGROUND

Breast cancer surpassed the prevalence of lung cancer in 2020, according to global cancer statistics, becoming the most common malignant tumor worldwide [1, 2]. Although the diagnosis and treatment of breast cancer substantially improved in recent decades, its prophylaxis and management are still an issue [3, 4].

Jumonji and the AT-rich interaction domain-containing 2 (JARID2) is a member of the Jumonji protein family; these proteins contain the Jumonji C (JmjC) domain and usually function as histone demethylases [5]. However, no demethylase activity of JARID2 has been detected due to the mutation of key amino acids in the catalytic domain of JARID2 [6]. JARID2 is an important regulator of embryonic stem cell gene expression, which is needed in the cellular signaling network that maintains pluripotency [7, 8]. Although the importance of JARID2 in embryonic stem cells has been determined, its role in the development and progression of solid tumors remains to be explored, especially in regards to breast cancer.

A study reported that embryonic stem cells with JARID2 deletion could not differentiate or exhibited delayed differentiation [9]. JARID2 bound to H2AK119ub1 in a process catalyzed by polycomb repressive complex 1 (PRC1) through its N-terminal ubiquitin interaction motif (UIM) [10]. JARID2 is a cofactor of PRC2; thus, it enhances the in vitro activity of the histone methyltransferase of PRC2 in the presence of H2AK119ub1-containing nucleosomes [11]. JARID2 bound to embryonic ectoderm development (EED) within PRC2, which allosterically activated it by methylation [12]. In addition, the combined presence of JARID2 and AE binding protein 2 (AEBP2) partially reduced the inhibition of PRC2 methyltransferase activity by post-translational histone modifications of H3K4me3 and H3K36me3 [13].

The nucleosome remodeling and deacetylase (NuRD) complex is one of the main types of chromatin remodeling complexes [14, 15]. In eukaryotes, it is firmly conserved and participates in multiple biological processes such as tumor progression, chromatin assembly, and genome stability [16]. The NuRD complex accelerated tumor progression by silencing various tumor suppressor genes (TSGs) via its deacetylase activity [17]. As the core subunit of the NuRD complex, metastasis-associated protein 1 (MTA1) is critical in shaping the NuRD complex [18]. Studies showed that the NuRD-PRC2 complex could mediate the dynamic balance between H3K27 methylation and acetylation in embryonic stem cells [14, 19]. The interplay between the NuRD complex and PRC2 has also been reported in breast cancer. A novel H3K27me2 reader, PHF20L1, cooperated with MTA1 in promoting breast tumorigenesis [20]. However, it remains unclear whether JARID2, the cofactor of PRC2, plays a role in the synergy between NuRD and the PRC2 complex in breast cancer.

Recently, metabolic reprogramming has been identified as one of the ten hallmarks of cancer [21]. Glycolysis and lipid metabolism are the two metabolic pathways enhanced in tumors; these changes provide energy support for cancer cells and promote the proliferation and metastasis of malignant tumors, including breast cancer [22]. Moreover, the production and utilization of energy in breast cancer are imbalanced, and this imbalance represents a non-neoplastic feature in the tumor microenvironment [23].

Obesity is one of the most conspicuous health concerns worldwide and confirmed as a risk factor for postmenopausal breast cancer [24]. In addition, obesity-specific cytokines, mainly leptin, are associated with some hallmarks of breast cancer, like increased cellular metabolism, sustained proliferative signaling, activated invasion, and metastasis [25]. Therefore, further research is essential to comprehend better the relationship between breast cancer and obesity. The prevalence of metabolic-related diseases, such as obesity, gradually increase each year. Dysregulated cellular metabolism, obesity and breast cancer are clearly linked [26]. Obesity can cause alterations in the metabolic pathways involved in the development and progression of breast cancer and in the microenvironment of breast tumors. However, the role which JARID2 has in this interplay between obesity and the metabolism of breast tumor, as well as its underlying mechanism, needs to be further investigated.

In this study, we mainly discussed the potential role of JARID2 in breast cancer and the latent association between its expression and adipocytes, with the purpose of expanding the future joint research of breast cancer and

obesity and laying an experimental basis for future drug development.

2 | MATERIALS AND METHODS

2.1 | Antibodies

The following antibodies were used in this study: anti-FLAG (1:100,000; F1408; Sigma-Aldrich, Burlington, MA, USA), anti-β-actin (1:200,000, A1978, Sigma-Aldrich), anti-leptin receptor (LEPR, 1:250, sc-8391, Santa Cruz Biotechnology, Santa Cruz, CA, USA), anti-signal transducer and activator of transcription 3 (STAT3, 1:1,000, sc-8019, Santa Cruz Biotechnology), anti-JARID2 (1:2,000, NB100-2214, Novus Biologicals, Minneapolis, MN, USA), anti-MTA2 (1:1,000, ab8106, Abcam, Cambridge, UK), anti-c-Myc (1:2,000, ab32072, Abcam), anti-SRY-box transcription factor 2 (SOX2, 1:1,000, ab97959, Abcam), anti-histone deacetylase 1 (HDAC1, 1:1,000, ab7028, Abcam), anti-POU class 5 homeobox1 (OCT4, 1:1,000, ab19857, Abcam), anti-HDAC2 (1:1,000, ab7029, Abcam), and anti-histone 3 (H3, ab127163, Abcam), anti-MTA1 (1:1,000, #5647S, Cell Signaling Technology, Danvers, MA, USA), anti-methyl-CpG binding domain protein 3 (MBD3, 1:1,000, #14540S, Cell Signaling Technology), anti-BRCA2 DNA repair associated (BRCA2, 1:1,000, #10741S, Cell Signaling Technology), anti-RB transcriptional corepressor 1 (RB1, 1:1,000, #9309S, Cell Signaling Technology), anti-inositol polyphosphate-4-phosphatase type II B (INPP4B, 1:1,000, #8450S, Cell Signaling Technology), anti-enhancer of zeste 2 (EZH2, 1:2,000, #5246S, Cell Signaling Technology), anti-KLF transcription factor 4 (KLF4, 1:2,000, #12173S, Cell Signaling Technology), anti-Nanog homeobox (NANOG, 1:1,000, #4903S, Cell Signaling Technology), anti-phospho-Stat3 (Ser727) (1:2,000, #9134T, Cell Signaling Technology), anti-phospho-Stat3 (Tyr705) (1:2,000, #9145S, Cell Signaling Technology), anti-p44/42 mitogen-activated protein kinase (MAPK, 1:1,000, #4695T, Cell Signaling Technology), anti-phospho-p44/42 MAPK (Thr202/Tyr204) (1:2,000, #9101S, Cell Signaling Technology), and anti-RB binding protein 7/4 (RbAp46/48, 1:1,000, #4633S, Cell Signaling Technology), anti-H3K27me3 (07-449, Millipore, Burlington, MA, USA), and anti-H3K27ac (07-360, Millipore). For the chromatin immunoprecipitation (ChIP) experiment, the following antibodies (2 μg for each sample) were used: anti-H3, anti-H3K27me3, anti-H3K27ac, anti-JARID2, anti-MTA1, anti-EZH2, anti-phospho-Stat3 (Tyr705), anti-phospho-p44/42 MAPK (Erk1/2) (Thr202/Tyr204) and anti-Phospho-Akt (Ser473) (#4060S; Cell Signaling Technology). Anti-JARID2 (1:100/1:300/1:500) was used to perform immunohistochemistry (IHC).

2.2 | Transfection and plasmid construction

Small hairpin RNAs (shRNAs) and endoribonuclease-prepared siRNAs (esiRNAs) were purchased from Sigma-Aldrich, while siRNAs were purchased from GenePharma, Shanghai, China. A JARID2 overexpression lentivirus (FLAG-JARID2) was generated to do the overexpression and rescue experiments. Briefly, lentiviruses for gene knockdown or overexpression were transfected using polybrene reagent (Sigma-Aldrich), and the infected cells were selected with puromycin. The esiRNAs and siRNAs for gene knockdown were transfected with Lipofectamine® RNAiMAX reagent (Invitrogen). All esiRNA, siRNA, and shRNA sequences used in this study are listed in Supplementary Tables S1-S2.

Complementary DNAs (cDNAs) were cloned into p3xFLAG-CMV-9, pCMV-Tag2B, pcDNA3.1-A, and pGL3-Basic plasmids, all purchased from Addgene, Watertown, MA, USA, and pGEX-4T-3 purchased from GE Life Sciences, Chicago, IL, USA. All the plasmids were verified by DNA sequencing, using the Sanger method. Plasmids were transfected with TurboFect (Thermo Fisher Scientific).

2.3 | Tissue specimens

A total of 6 pairs of breast cancer tissues and adjacent normal tissues were obtained from patients diagnosed with breast cancer during Jan-Feb 2022 at Cancer Hospital, Chinese Academy of Medical Sciences (Beijing, China). All samples were frozen in liquid nitrogen immediately after surgical resection. Clinical characteristics of patients are described in Supplementary Table S3.

2.4 | Cell culture and coculture assays

Human breast cancer cell lines (MCF-7, T-47D, BT-474, MDA-MB-231, Hs 578T and MDA-MB-468), human non-malignant breast epithelial cells (MCF-10A), and human embryonic kidney cells (HEK293T) were originated from the American Type Culture Collection (ATCC, Manassas, VA, USA).

MDA-MB-231 cells were cultured in an L-15 medium (Cytiva) containing 10% fetal bovine serum (FBS, Gbico, Invitrogen) without CO_2 at 37°C. MCF-10A cells were cultivated in mammary epithelium basal medium (MEBM) supplemented with bovine pituitary extract, human recombinant epidermal growth factor (hEGF), insulin, hydrocortisone and GA-1000 (Lonza, Basel, Switzerland) in 5% CO_2 at 37°C. In addition, other cells were cultivated in Dulbecco's modified Eagle's medium (DMEM,

Biological Industries, Beit HaEmek, Israel) containing 10% FBS and 5% CO_2 at 37°C.

Human preadipocytes (Zhejiang Meisen Cell Technology Co., Ltd., Jinhua, Zhejiang, China) were cultured and differentiated according to the following procedure. After reaching 90% confluence, human preadipocytes were digested with trypsin-ethylenediaminetetraacetic acid (EDTA, Gibco, Invitrogen), and the resuspended cells were inoculated in 6-well plates (BIOFIL, Guangzhou, Guangdong, China). Approximately 2 days after reaching contact inhibition, differentiation of preadipocytes was induced by their culture in a specific DMEM medium containing 10% FBS, 10 μg/mL insulin (Solarbio, Beijing, China), 0.5 mmol/L isobutylmethylxanthine (Solarbio), and 1 μmol/L dexamethasone (Solarbio) for 2 days. Then the medium was replaced with a special DMEM medium with 10% FBS and 10 μg/mL insulin. After 2 days, the medium was replaced with a normal DMEM medium with 10% FBS. After 12 days, Oil red O staining (Solarbio) was used to verify differentiation efficiency.

The coculture assay was implemented in the following ways. Preadipocytes (1×10^5 cells/well) were planted in the lower chamber of a 24-well plate (BD Biosciences, Franklin Lakes, NJ, USA), induced and differentiated for 12 days as described above; breast cancer cells (5×10^4 cells/well) were further placed in the upper transwell chamber (Corning, Corning, NY, USA) to form a coculture with adipocytes. To evaluate the influence of adipocytes on the invasion of breast cancer cells, after 18-24 h of coculture, we stained the lower side cells with crystal violet, wiped off the upper side cells with cotton swabs, and counted the cells with the ImageJ software (National Institutes of Health, NIH, Bethesda, MD, USA). For each membrane, three independent fields were selected for counting.

Human patient-derived primary breast cancer cells (M-CH1199, Shanghai Mcellbank Biotechnology Co., Ltd, Shanghai, China) were cultivated in DMEM/F12 (M-CH1199-500, Shanghai Mcellbank Biotechnology Co., Ltd) containing specific additives [basic fibroblast growth factor (bFGF), insulin, ascorbic, L-glutamine, and hEGF], 1% penicillin/streptomycin, 10% FBS and 5% CO_2 at 37°C. The remaining culture conditions were the same as those used for HEK293T cells.

The appropriate conditions and duration of leptin treatment were explored. Cells were starved in serum-free medium for 16 h, synchronized, and then similarly treated with different concentrations of leptin (H0317, PEPROTECH, Thermo Fisher Scientific, Waltham, MA, USA), PD98059 (an MAPK/ERK inhibitor, S1177), LY294002 [a phosphoinositide 3-kinase (PI3K) inhibitor, S1105], FLLL32 [a Janus kinase 2/signal transducer and activator of transcription 3 (JAK2/STAT3) inhibitor, S7259] purchased from Selleckchem, Houston, TX, USA or Colivelin (an agonist) purchased from MedChemExpress, Monmouth Junction, NJ, USA.

2.5 | RNA-sequencing (RNA-seq) and real-time quantitative PCR assay (RT-qPCR)

For RNA-seq, total RNA from MDA-MB-231 cells infected with shJARID2#2 or shSCR lentivirus was extracted using TRIzol reagent (Invitrogen). RNA quality was checked using Agilent 2100 Bioanalyzer (Agilent Technologies). Then RNA libraries were prepared for sequencing using standard capital biotech protocols. Trimmomatic (version: v0.39) was used for filter reads, and Hisat2 (version: v2.0.4) was used to map clean reads to a reference genome (hg38) using the default parameters. The genome sorted BAM file was indexed using Samtools (version: v1.7). We used the fragments per kilobase per million mapped fragments (FPKM) method and featureCounts (version: v2.0.1) to calculate the level of expression of genes. DESeq2 was used to determine differentially expressed genes (DEGs) ($P < 0.001$ and |fold change| > 1.5). The Kyoto Encyclopedia of Genes and Genomes (KEGG, http://david.ncifcrf.gov/) and Gene Set Enrichment Analysis (GSEA, version: v4.2.3) were used to perform pathway analysis. The aforementioned raw data are available at www.ncbi.nlm.nih.gov/geo/query/acc.cgi?acc = GSE202868.

For the RT-qPCR assay, TRIzol reagent was used to extract total RNA. DNase/RNase-free water (Solarbio) was used to dissolve it and eliminate DNA contamination. Then cDNA was prepared using TranScript One Step cDNA Synthesis SuperMix Kit (TransGen, Beijing, China). TransStart Top Green qPCR SuperMix (TransGen) and ABI PRISM 7500 FAST Sequence Detection System (Applied Biosystems, Waltham, MA, USA) were used to detect all transcripts, and quantitation of gene expression was performed applying the comparative CT method ($2^{-\Delta\Delta CT}$). Actin beta (ACTB) was used as an internal reference gene. Each test was performed three times. All primer sequences are listed in Supplementary Table S4.

2.6 | Mass spectrometry

HEK293T cells were transfected with FLAG-tagged JARID2 and incubated for 48 h. Anti-FLAG M2 affinity gel (A2220, Sigma-Aldrich, Burlington, MA, USA) was then used to prepare the anti-FLAG immune affinity columns. Approximately 4×10^8 cells were used to prepare cell lysates. The lysates were placed in a balanced flag column to allow the protein complex to bind to

the column resin. Next, the column was washed with a special cold buffer (500 mmol/L KCl, 2 mmol/L EDTA, 10% glycerol, 50 mmol/L Tris, complete phosphatase and protease inhibitor cocktails), and the FLAG peptide (0.2 mg/mL, F4799, Sigma-Aldrich) was used to elute the FLAG protein complex. The proteins were separated using Nu-polyacrylamide gel electrophoresis (Nu-PAGE). Data obtained after silver staining and mass spectrometry sequencing were analyzed.

2.7 | Co-immunoprecipitation and Western blotting

For co-immunoprecipitation (co-IP) experiments, cells were washed with cold phosphate-buffered saline (PBS) three times. Cells were treated with a specific lysis buffer containing 150 mmol/L NaCl, 0.5% NP-40, complete phosphatase and protease inhibitor cocktails (04693132001, Roche, Basel, Switzerland), 50 mmol/L Tris-HCl, 1 mmol/L EDTA, and 0.25% sodium deoxycholate for 1 h at 4°C. Next, the lysates were centrifuged at 13,523 × *g* and 4°C for 15 min in a centrifuger (Eppendorf 5424R). The corresponding primary antibodies were added to the cell extracts, and the mixture was shaken overnight at 4°C. Dynabeads™ Protein G (10004D, Invitrogen, Carlsbad, CA, USA) was added to the mix, which was gently shaken for 2 h at 4°C. Next, cell lysis buffer was used to wash Protein G beads five times at 4°C. Sodium dodecyl sulfate-polyacrylamide gel electrophoresis (SDS-PAGE) was performed to separate the obtained conjugate. After incubation with secondary antibodies, detection of proteins was performed using an enhanced chemiluminescence (ECL System).

2.8 | GST pull-down assays

GST-fusion constructs were expressed in *Escherichia coli* BL21 cells (C504-02/03, Vazyme, Nanjing, Jiangsu, China). Crude bacterial lysates were prepared by sonicating the cells in PBS containing a protease inhibitor cocktail at 4°C. Then 30 μL Glutathione Sepharose™ 4B beads (17075601, Cytiva, Marlborough, MA, USA) were added to the mixture and blended at 4°C for 2 h, to purify the GST-fusion proteins. T3 coupled reticulocyte lysate system (L4950, Promega, Madison, WI, USA) and T7 quick coupled transcription/translation system (L1170, Promega) were used to conduct the in vitro transcription and translation assays. In total, 10 μL mix of transcription/translation products and approximately 10 μg of corresponding GST-fusion protein were incubated at 25°C with a special buffer (containing 0.8% bovine serum albumin and a protease inhibitor cocktail in PBS) for 30 min. The 4B beads were washed five times, and 30 μL loading buffer was added. Beads were boiled at 95°C for 10 min. SDS-PAGE was conducted to separate the obtained conjugate. Western blotting was used to detect protein bands after treatment with specific antibodies.

2.9 | Luciferase reporter assays

For luciferase reporter assays, promoter fragments of the genes of interest were designed, inserted into pGL3-basic plasmids and co-transfected with the substrates into HEK293T cells. After 48 h, the cells were taken out. Dual-luciferase kit (E1910, Promega) was used to detect luciferase activity in accordance with the manufacturer's instructions. Each test was conducted three times.

2.10 | ChIP-seq, qChIP, and Re-ChIP assays

For ChIP experiments, approximately 5×10^7 MDA-MB-231 cells were collected, crosslinked with formaldehyde, sonicated, and centrifuged at 13,523 × *g* and 4°C for 15 min. The supernatant was collected, then treated with 2 μg of the corresponding ChIP grade antibodies; the mix was incubated at 4°C overnight. Next, 10 μL Dynabeads™ Protein G was added, and the mix was incubated at 4°C for 4 h. The beads were cleaned sequentially with specific low- and high-salt ChIP wash buffers. De-crosslinking was performed by incubating the eluent at 65°C overnight. Finally, the enriched DNA was recovered with NucleoSpin Gel and PCR Clean-up Kit (740609, MACHEREY-NAGEL, Düren, North Rhlne-Westphalia, Germany).

For qChIP experiments, TransStart Top Green qPCR SuperMix was used to detect enrichment status.

For Re-ChIP experiments, 20 mmol/L dithiothreitol was used to elute the immune complex. ChIP dilution buffer was used to dilute the eluent. A second ChIP reaction was performed. The beads were eluted with Tris-EDTA buffer containing 1% SDS. DNA recovery steps were the same as those in ChIP experiments. The enriched DNA template was detected by conventional PCR.

For ChIP-seq experiments, the TruePrep DNA Library Prep Kit (Vazyme) was used to conduct DNA library construction. ChIP-seq was performed by CapitalBio Technology, Beijing, China. Basecall files were generated using Illumina BCL2fastq version v1.8.4. Data were filtered using the NGS QC Toolkit version v2.3.3. High-quality reads were aligned against the human genome (hg19) using Bowtie (version 0.12.8). The expression peaks were analyzed using model-based analysis for ChIP-Seq. ChIPseeker was used to determine the genomic distribution of JARID2-binding

sites. Motif analysis was conducted using Multiple Em for Motif Elicitation (https://meme-suite.org/meme/).

ChIP-seq dataset is available at www.ncbi.nlm.nih.gov/geo/query/acc.cgi?acc=GSE202867. All qChIP primer sequences are listed in Supplementary Table S5.

2.11 | Colony formation and cell invasion assays

For colony formation assays, cells (5,000 cells/well) were seeded and cultured in 6-well plates for approximately 14 days. Afterwards, cells were stained with crystal violet.

For cell invasion assays, transwell chamber filters were coated with Matrigel matrix (BD Biosciences, Franklin Lakes, NJ, USA). Cells were resuspended with serum-free medium; 2-4 $\times 10^4$ cells were put into the upper chamber of the transwell plates. In total, 500 μL culture medium with 10% FBS was placed into the lower chamber and incubated at 37°C for 18-24 h. Crystal violet was used to stain cells in the lower chamber. To evaluate the efficiency of the invasion, the cells on the filters of the upper transwell chamber were wiped with cotton swabs. Stained cells were counted with ImageJ. For each membrane, three independent regions were selected for counting.

2.12 | Second-generation sphere formation assays

For first-generation sphere formation, 0.5×10^4 cells were cultivated in ultra-low attachment plates with DMEM/F12 culture medium (Gbico) containing 20 ng/mL bFGF, B-27 (Invitrogen), 0.4% bovine serum albumin, 5 μg/mL insulin (Invitrogen), and 10 ng/mL hEGF, without serum supplementation [27]. The diameters and numbers of spheres were measured and counted at day 15. The first-generation spheres were then collected and centrifuged at 60 $\times$ *g* and 25°C for 4 min. The precipitated cells were digested with trypsin and counted. The same experimental steps were repeated to obtain second-generation spheres.

2.13 | Extracellular acidification rate (ECAR), free fatty acid (FFA), and triglyceride (TG) detection

The ECAR was determined using a Seahorse XF Glycolysis Stress Test Kit (103020-100, Agilent Technologies, Santa Clara, CA, USA) according to the instructions of the manufacturer and analyzed using a Seahorse XFe24 Extracellular Flux Analyzer (Seahorse Bioscience, North Billerica, MA, USA).

The concentrations of FFA (BC0595, Solarbio) and TG (BC0625, Solarbio) were determined using the corresponding kits as indicated in their instructions.

2.14 | Mouse xenograft models

To evaluate the in vivo tumor formation capacity, MDA-MB-231 cells, infected with shSCR or shJARID2 lentivirus, were mixed with Matrigel matrix and injected at various cell numbers (5×10^3, 1×10^3, 5×10^2, or 100 cells) into the mammary fat pads of 6-week-old NOD/SCID female mice ($n = 6$, Vital River Laboratory Animal Technology, Beijing, China). Tumor growth was gauged continuously for 2 months. The tumor volume was calculated by the formula: volume = 0.5 $\times$ length $\times$ width^2. Tumors grew to a maximum of 10% of the animal's original weight, and their average diameter did not exceed 20 mm. Mice were euthanized using cervical dislocation. Extreme limiting dilution analysis (ELDA) was used to calculate the frequency of tumor-initiating cells [28]. ELDA is suitable for any limiting dilution problem, but special methods are implemented to give reliable results in extreme data situations. The calculations were performed at this website: https://bioinf.wehi.edu.au/software/elda/index.html.

2.15 | Immunohistochemical staining

JARID2 expression in tumor and marginal tissues of multiple organs (the breast, bladder, colon, liver, kidney, lung, esophagus) was determined by IHC (Alena Biotechnology, Xi'an, Shaanxi, China). This experimental work was largely completed by Alena Biotechnology. In brief, the following steps were performed: slices were maintained at 60°C for 30 min, dewaxed and hydrated; the antigen was retrieved; the endogenous peroxidase was blocked with H_2O_2; non-immune animal serum was added at 25°C; JARID2 antibody (1:500) was added, and the mix was refrigerated at 4°C overnight; sheep anti-mouse/rabbit IgG was added; streptomyces avidin peroxidase was added; we performed staining with diaminobenzidine (DAB) for 5 min and counterstaining with hematoxylin; the slices were then dehydrated and sealed with neutral gum.

The evaluation criteria for IHC experiments were as follows. The samples were considered invalid if the samples were short of grade information, paraffin sections were curling or not the indicated tissues after IHC staining. In regards to color: no color was negative (-), shades of light brown were weakly positive (+), shades of brown were positive (++), and shades of tan were strongly positive (+++); in regards to the proportion of positive cells: the proportion under 25% (+), the proportion between 25% and 50% (++),

and the proportion above 50% (+++). Finally, the color intensity results were based on the combined evaluation of these two results.

2.16 | 5-ethynyl-2-deoxyuridine (EdU) assays

EdU staining was performed using Cell-Light EdU Apollo®567 In Vitro Kit (C10310-1, RiboBio, Guangzhou, Guangdong, China) according to the manufacturer's protocol. We first put the slides in 6-well plates, and then cells (2×10^5 cells/well) were seeded and cultured. Next, we followed the procedure from manufacturer's instructions to detect EdU-labeled positive cells.

2.17 | Flow cytometry

For flow cytometry experiments, BT-474 or Hs 578T cells were transfected with lentivirus-delivered Vector or FLAG-JARID2, and control or JARID2-targeting esiRNAs. Then the cells were synchronized to G0 phase with serum deprivation for 24 h. After incubated in normal medium for 12 h, the cells were fully digested by pancreatin and collected by low-speed centrifugation at 94 × *g* and 25°C for 3 min, then the cells were treated with 70% cold ethanol and fixed under -20°C condition for more than 12 h. The cells were centrifuged at 94 × *g* and 4°C for 3 min, washed slightly with PBS and resuspended, incubated with RNase A (Sigma-Aldrich) for 30 min at 25°C. Finally, the cells were incubated with propidium iodide (Sigma-Aldrich) for 30 min at 25°C. Single-cell suspensions were analyzed using a flow cytometer (BD Biosciences), processed with CellQuest™ Pro software (BD Biosciences). Each test was performed at least three times.

2.18 | Bioinformatics

The cancer databases used in this paper were downloaded from The Cancer Genome Atlas (TCGA) (http://www.cancer.gov/about-nci/organization/ccg/research/structural-genomics/tcga) and Gene Expression Omnibus (GSE42568, GSE32641, GSE62931, GSE9195, GSE58812 and GSE104549 for breast cancer, GSE17025 for endometrial cancer and GSE51062 for glioblastoma, https://www.ncbi.nlm.nih.gov/geo/). These datasets were used to evaluate the expression of JARID2 and the correlation between JARID2 and breast cancer prognosis.

The Kaplan-Meier survival analysis was utilized to examine the relationship between JARID2 expression and survival of patients with breast cancer in TCGA and GEO datasets (GSE42568, GSE9195 and GSE58812). Published clinical datasets (GSE9195 and GSE58812) were analyzed using Kaplan-Meier survival analysis and log-rank test to determine the differences in overall survival (OS), relapse-free survival (RFS), distant metastasis-free survival (DMFS), and metastasis-free survival (MFS) by JARID2 and MTA1 status. OS and MFS were defined from diagnosis to death/last follow-up or first metastasis. RFS and DMFS were calculated as the interval between diagnosis and first locoregional relapse or the first distant metastasis.

Several databases related to transcription factors were used to investigate the transcription factor in volved in JARID2 expression regulation: CHEA Transcription Factor Target (https://maayanlab.cloud/Harmonizome/dataset/CHEA+Transcription+Factor+Targets), ENCODE Transcription Factor Target (https://maayanlab.cloud/Harmonizome/dataset/ENCODE+Transcription+Factor+Targets), JASPAR Predicted Transcription (https://maayanlab.cloud/Harmonizome/dataset/JASPAR+Predicted+Transcription+Factor+Targets), and hTFtarget (http://bioinfo.life.hust.edu.cn/hTFtarget#!/).

2.19 | Statistical analysis

The mean ± standard deviation (SD) was used to process the data unless otherwise stated. The differences between the groups were analyzed with either the two-tailed unpaired *t*-test or one-way analysis of variance (ANOVA) test using SPSS statistics 27.0 software (IBM, Armonk, NY, USA).

3 | RESULTS

3.1 | JARID2 was upregulated in breast cancer and promoted carcinogenesis of breast cancer cells

To understand the role of JARID2 in breast cancer progression, we collected 142 breast tumor tissues and 8 adjacent normal tissues and detected JARID2 expression using IHC microarrays. After removing 8 invalid tumor samples, JARID2 expression was shown to be significantly upregulated in breast cancer and associated with the histological grade (Figure 1A). In addition, analysis of TCGA and GEO datasets (GSE42568, GSE32641, and GSE62931) indicated that the expression of JARID2 was higher in breast tumor tissues than in adjacent normal tissues (Figure 1B). Moreover, these results were confirmed by Western blotting in 6 paired breast cancer and adjacent normal tissue samples (Supplementary Figure S1A). Using Kaplan-Meier survival analysis of TCGA and GEO datasets, we showed that in

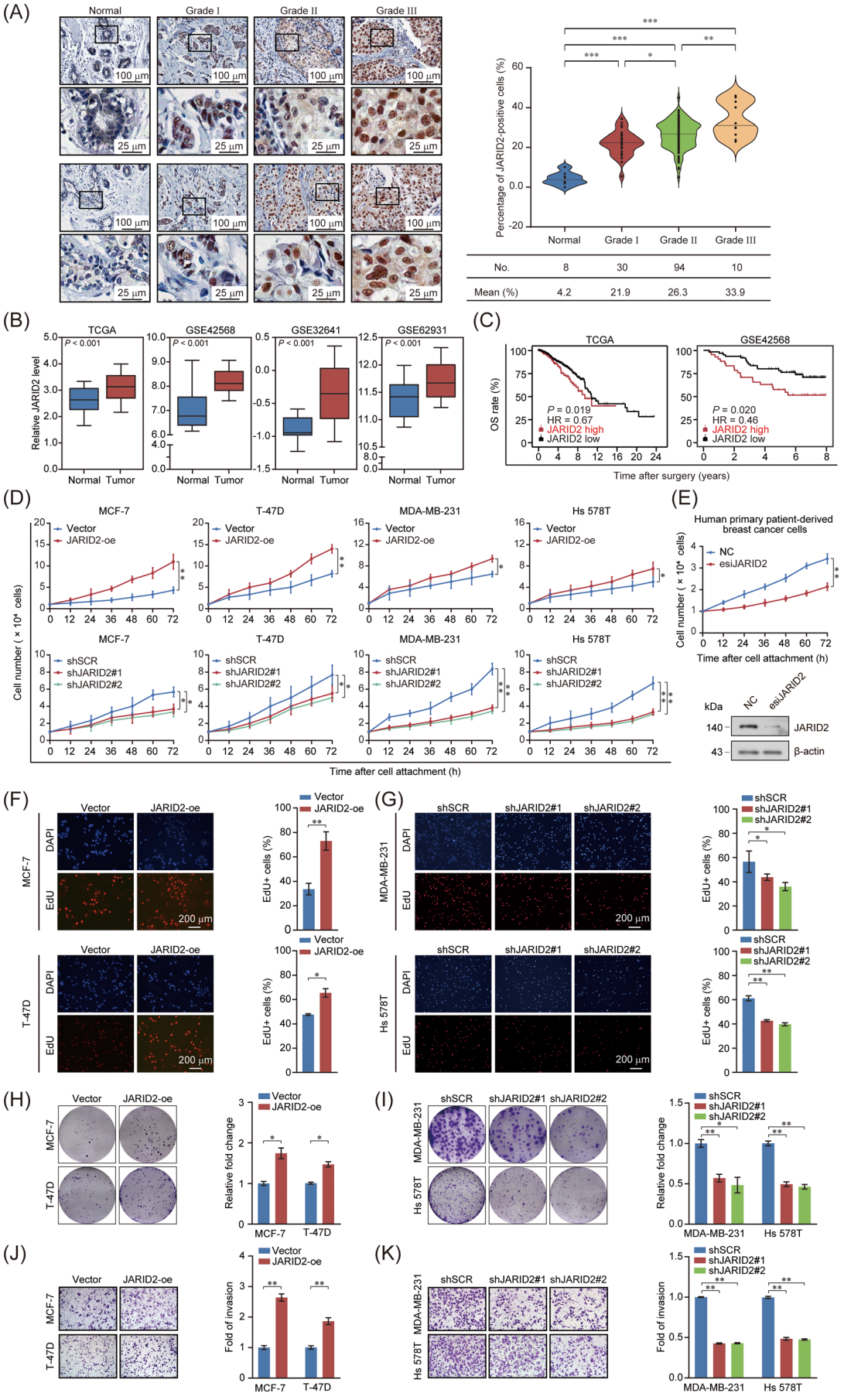
(A)
Normal
Grade I
Grade II
Grade III
100 μm
25 μm
Percentage of JARID2-positive cells (%)
No. 8 30 94 10
Mean (%) 4.2 21.9 26.3 33.9
(B)
TCGA
GSE42568
GSE32641
GSE62931
P < 0.001
Relative JARID2 level
Normal Tumor
(C)
TCGA
GSE42568
OS rate (%)
P = 0.019
HR = 0.67
P = 0.020
HR = 0.46
JARID2 high
JARID2 low
Time after surgery (years)
(D)
MCF-7
T-47D
MDA-MB-231
Hs 578T
Vector
JARID2-oe
shSCR
shJARID2#1
shJARID2#2
Cell number (× 10⁴ cells)
Time after cell attachment (h)
(E)
Human primary patient-derived breast cancer cells
NC
esiJARID2
Cell number (× 10⁴ cells)
Time after cell attachment (h)
kDa
140
43
JARID2
β-actin
(F)
Vector
JARID2-oe
DAPI
EdU
200 μm
EdU+ cells (%)
(G)
shSCR
shJARID2#1
shJARID2#2
(H)
Relative fold change
(I)
(J)
Fold of invasion
(K)

patients with breast cancer, a higher level of expression of JARID2 was related to poor prognosis (Figure 1C).

To further evaluate the role of JARID2 in breast cancer development, the baseline level of expression of JARID2 was determined in different breast cancer cell lines by Western blotting. The results showed that the expression level of JARID2 was higher in highly invasive cell lines (MDA-MB-231, Hs 578T, MDA-MB-468) than in low invasive breast cancer cell lines (MCF-7, T-47D, BT-474) (Supplementary Figure S1B). MCF-7, T-47D, MDA-MB-231, and Hs 578T cells were used to generate JARID2 overexpression or knockdown cells (Supplementary Figure S1C-D). Furthermore, JARID2 overexpression promoted breast cancer cell proliferation, whereas knockdown of JARID2 significantly inhibited cell proliferation (Figure 1D). Thus, to investigate the role of JARID2 in breast cancer, JARID2 was overexpressed in luminal type MCF-7 and T-47D cells, and deleted in triple-negative breast cancer (TNBC) MDA-MB-231 and Hs 578T cells. Meanwhile, in order to imitate the physiological environment of breast cancer tissues, we also used human patient-derived primary breast cancer cells. We transfected the primary breast cancer cells with esiRNA targeting JARID2. Using a growth curve experiment, we determined whether JARID2 knockdown inhibited the tumorigenesis of breast cancer cells. The results showed that the knockdown of JARID2 in primary breast cancer cells inhibited cell proliferation (Figure 1E). Next, an EdU experiment was used to confirm the growth-promoting effect of JARID2. Compared to control cells, the results showed a much higher proportion of EdU-labeled cells in JARID2-overexpressing MCF-7 and T-47D cells and a lower proportion of EdU-labeled cells in JARID2-knockdown MDA-MB-231 and Hs 578T cells (Figure 1F-G). A colony formation assay was performed to confirm the above results (Figure 1H-I). Moreover, results from the transwell experiments implied that JARID2 overexpression markedly enhanced the invasion of MCF-7 and T-47D cells, while JARID2 knockdown in MDA-MB-231 and Hs 578T cells weakened this phenomenon (Figure 1J-K). Consistent with the above results, knockdown of JARID2 expression significantly decreased the proliferation and invasion in HER2-positive BT-474 cells (Supplementary Figure S2A-C), whereas overexpression of JARID2 under the same genetic background enhanced the proliferation and invasion ability in BT-474 and Hs 578T cells (Supplementary Figure S2D-F). Also, JARID2 overexpression decreased the cell number of the G1 phase and increased the cell numbers of the S and G2/M phases in BT-474 and Hs 578T cells, while knockdown of JARID2 exhibited the opposite effect (Supplementary Figure S2G-H). In short, JARID2 was upregulated in breast cancer and enhanced the proliferation and invasion of breast cancer cells.

3.2 | JARID2 promoted the stemness of breast cancer cells

To further investigate the function of JARID2 in breast cancer development, increased mRNA and protein levels of "stemness" marker genes (*OCT4*, *KLF4*, *SOX2*, *c-Myc*, and *NANOG*) were detected in MCF-7 and T-47D breast cells overexpressing JARID2, whereas JARID2 knockdown in MDA-MB-231 and Hs 578T cells reduced these levels (Figure 2A-B). Moreover, second-generation sphere formation assays showed that overexpression of JARID2 led to increased sphere-forming efficiency and sphere diameter compared with control cells, while JARID2 knockdown had opposite consequences (Figure 2C-F). Similarly, the results of the first-generation sphere formation assays showed that the number and size of spheres increased in MCF-7 and T-47D cells overexpressing JARID2, while decreased in MDA-MB-231 and Hs 578T cells with JARID2

FIGURE 1 JARID2 was upregulated in breast tumor and fostered breast tumor carcinogenesis. (A) In normal breast tissue and breast tumor tissues, the immunohistochemical staining of JARID2 was analyzed from the perspective of histological grades (I, II, and III). One-way ANOVA was used to analyze the difference between positive stained nuclei in the samples. (B) The public datasets on JARID2 expression (TCGA, GSE42568, GSE32641, and GSE62931) were analyzed using two-tailed unpaired *t*-test. (C) The relationship between JARID2 expression and survival time in breast tumor was analyzed using the Kaplan-Meier survival method with TCGA or GSE42568 datasets. (D) To perform growth curve analysis, MCF-7, T-47D, MDA-MB-231, and Hs 578T cells were infected with lentivirus containing overexpressed (vector and FLAG-JARID2) or knocked down (shSCR and shJARID2) JARID2. (E) Human patient-derived primary breast cancer cells were transfected with esiRNAs targeting NC or JARID2 to perform growth curve analysis. The expression of JARID2 was detected by Western blotting. β-actin was used as an internal reference protein. (F-G) EdU was incubated with treated MCF-7, T-47D, MDA-MB-231, and Hs 578T cells for 2 h. EdU was detected using a fluorescence microscope. (H-I) Before crystal violet staining, treated MCF-7, T-47D, MDA-MB-231, and Hs 578T cells were cultured in the medium for a week. Representative pictures were displayed and analyzed. (J-K) We used the corresponding lentivirus to transfect MCF-7, T-47D, MDA-MB-231, and Hs 578T cells and performed transwell invasion assays. Invading cells were stained with crystal violet and counted by ImageJ. (B, D-J) Error bars indicate means ± SD. The data was analyzed by two-tailed unpaired *t*-test, $^{*}P < 0.05$, $^{**}P < 0.01$, $^{***}P < 0.001$.

Abbreviations: IHC, immunohistochemistry; TCGA, The Cancer Genome Atlas; GEO, Gene Expression Omnibus; HR, hazard ratio; OS, overall survival; shSCR, scramble; oe, overexpression; esiRNA, endoribonuclease-prepared siRNA; NC, negative control; EdU, 5-ethynyl-2-deoxyuridine; DAPI, 4,6-diamidino-2-phenylindole.

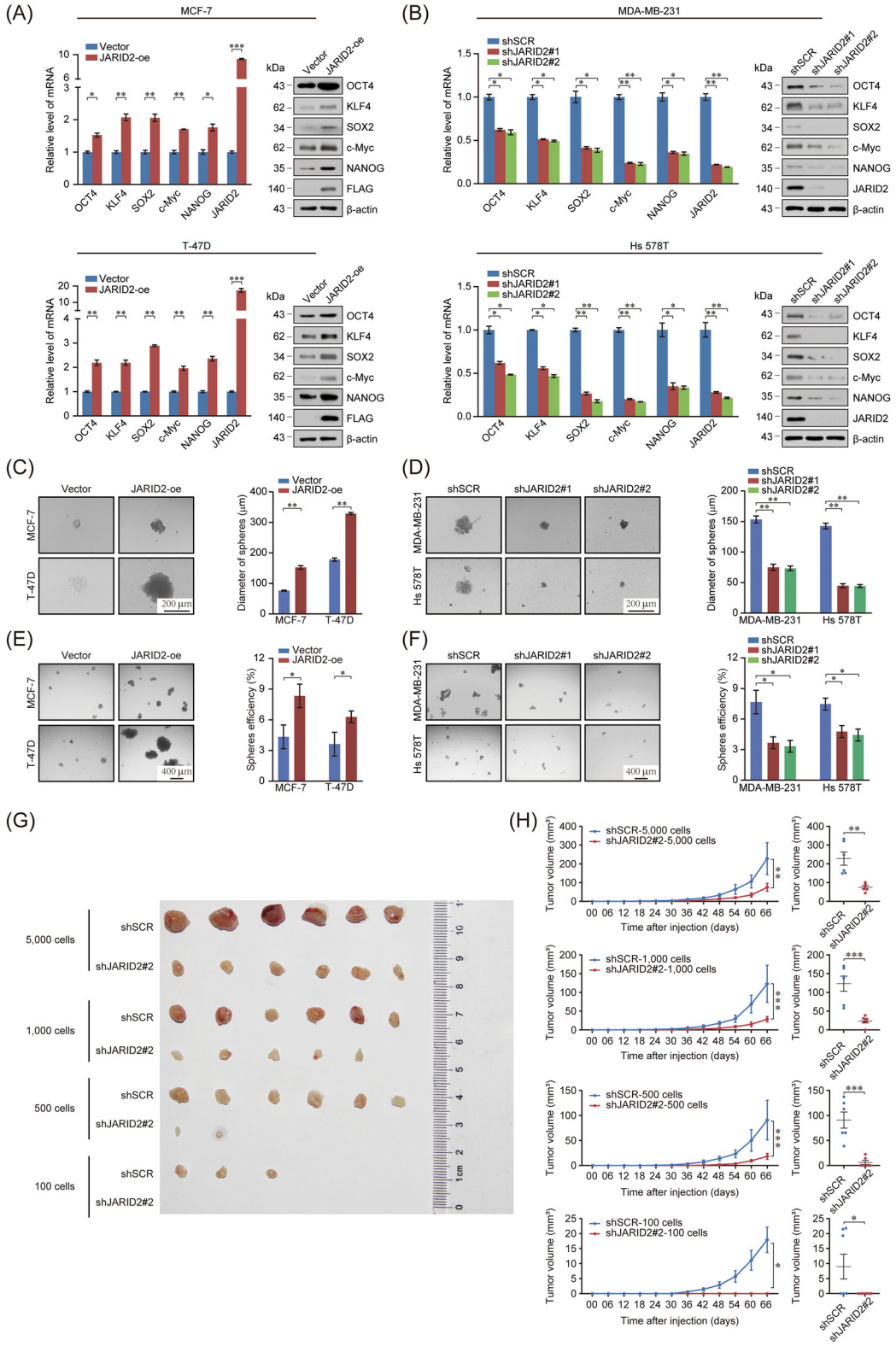

FIGURE 2 JARID2 promoted the maintenance of breast cancer stemness in vivo and in vitro. (A-B) The expression of stem cell markers was detected using Western blotting and RT-qPCR in breast cancer cells infected with lentivirus containing overexpressed JARID2 (vector, and FLAG-JARID2) or knocked down JARID2 (shSCR, and shJARID2). ACTB was used as an internal reference gene for assessing mRNA level; β-actin was used as an internal reference protein for Western blotting. (C-F) The second-generation sphere formation assay was performed in MDA-MB-231, Hs 578T, MCF-7, and T-47D cells. The number and diameter of spheres were quantified. (G-H) For xenograft tumors assay, MDA-MB-231 cells infected with shSCR or shJARID2#2 lentivirus were injected at various cell numbers to NOD/SCID mice (n = 6). The tumorigenicity was evaluated by measuring the tumor growth. In the specified time period, the tumor growth curve was determined

knockdown (Supplementary Figure S3). These results indicated that JARID2 was associated with stemness maintenance in breast cancer cells.

To further estimate the role of JARID2 in the frequency of breast cancer stem cells (CSCs) in vivo, we constructed a xenograft mouse model in NOD/SCID mice. The frequency of CSCs was significantly lower in the JARID2-knockdown group than in the control group (Supplementary Table S6). Furthermore, in the shSCR group, mice developed tumors with as few as 100 cells, while in the shJARID2#2 group, mice presented no tumors (Figure 2G), indicating that the probability of tumor formation was appreciably lower after JARID2 knockdown than in its presence. The tumor growth rate was significantly inhibited in the shJARID2#2 group (Figure 2H). These results suggested that JARID2 significantly promoted the stemness of breast cancer cells.

3.3 | JARID2 regulated the expression of target genes related with tumor suppression, glycolysis, and lipid metabolism

To determine how JARID2 regulates the development of breast cancer, RNA-seq experiments were conducted in MDA-MB-231 cells infected with scramble or JARID2-knockdown lentivirus. Compared with the control group, we identified 2,204 upregulated and 2,689 downregulated genes in JARID2 knockdown cells (Figure 3A, left). The KEGG analysis revealed that downregulated genes were enriched in pathways regulating cell adhesion, glycolysis/gluconeogenesis, fatty acid metabolism, hypoxia, MYC, and epithelial-mesenchymal transition (EMT), whereas upregulated genes were enriched in pathways associated with oxidative phosphorylation, G2-M checkpoint, and DNA damage repair (Figure 3A, right). Loss of function of TSGs can induce carcinogenesis [29, 30]. Analyzing the role of JARID2 on the occurrence and development of breast cancer cells, we discovered that the knockdown of JARID2 could upregulate the expression of many TSGs, such as *INPP4B*, *BRCA2*, and *RB1* (Supplementary Figure S4). These results were then confirmed by RT-qPCR in MDA-MB-231 and Hs 578T cells (Figure 3B).

Next, we discovered that the glycolysis/gluconeogenesis and oxidative phosphorylation pathways were enriched using GSEA (Figure 3C). Tumor cells exert the Warburg effect, which is associated with impairment of mitochondrial oxidative phosphorylation, abnormal expression of glucose metabolic enzymes, oncogene activation, TSG inactivation, and changes in the tumor microenvironment [31]. Consistent with this, several glycolysis-related genes such as hexokinase 2 (*HK2*), phosphoglycerate kinase 1 (*PGK1*), and lactate dehydrogenase A (*LDHA*), were downregulated in the JARID2-depleted cells (Figure 3D). RT-qPCR analysis confirmed the downregulation of 10 glycolysis-related genes in MDA-MB-231 and Hs 578T cells with JARID2 depletion (Figure 3E). Furthermore, a reduction in the expression levels of PGK1 and LDHA was observed in cells transfected with shJARID2#2, as confirmed by Western blotting (Figure 3F). In breast cancer cells, glycolysis was measured in MDA-MB-231 and Hs 578T cells using the Seahorse XFe24 Extracellular Flux Analyzer. Our results showed that deletion of JARID2 significantly decreased glycolysis levels (Figure 3G). The efficiency of esiRNA targeting JARID2 was verified in MDA-MB-231 and Hs 578T cells (Supplementary Figure S5). RNA-seq indicated that the expression of many lipid metabolism-related genes, including fatty acid desaturase 2 (*FADS2*), glyceraldehyde-3-phosphate dehydrogenase (*GAPDH*), and sterol regulatory element binding transcription factor 1 (*SREBF1*), was decreased in JARID2-deficient cells (Figure 3H). The expression of 10 lipid metabolism-related genes was down-regulated in JARID2-deficient MDA-MB-231 and Hs 578T cells (Figure 3I). Simultaneously, we found that the levels of FFA and TG were decreased after JARID2 knockdown in MDA-MB-231 and Hs 578T cells (Figure 3J-K). In brief, these results suggested that JARID2 could restrain the expression of TSGs, such as *BRCA2*, *RB1*, and *INPP4B*, and upregulate the expression of glycolysis- and lipid metabolism-related genes, influencing glycolysis and lipid metabolism.

3.4 | JARID2 was physically linked to the NuRD complex

To better understand the mechanism underlying the effect of JARID2, proteins interacting with it were identified by affinity purification and mass spectrometry in HEK293T cells. As reported by many groups[12, 32], components of the PRC2 complex, polycomb repressive complex 2 subunit (SUZ12), EED, EZH2, and RbAp46/48, were co-purified with JARID2 (Figure 4A-B). Besides the previously

and tumor volume data were detected at the end point. The data was processed with mean ± SEM and analyzed by two-tailed unpaired *t*-test, $^{*}P < 0.05$, $^{**}P < 0.01$, $^{***}P < 0.001$. (A-F) The data was analyzed by two-tailed unpaired *t*-test, $^{*}P < 0.05$, $^{**}P < 0.01$, $^{***}P < 0.001$.

Abbreviations: CSC, cancer stem cell; shSCR, scramble; oe, overexpression; NOD/SCID, Non-obese diabetic/severe combined immune deficiency; ELDA, Extreme Limiting Dilution Analysis.

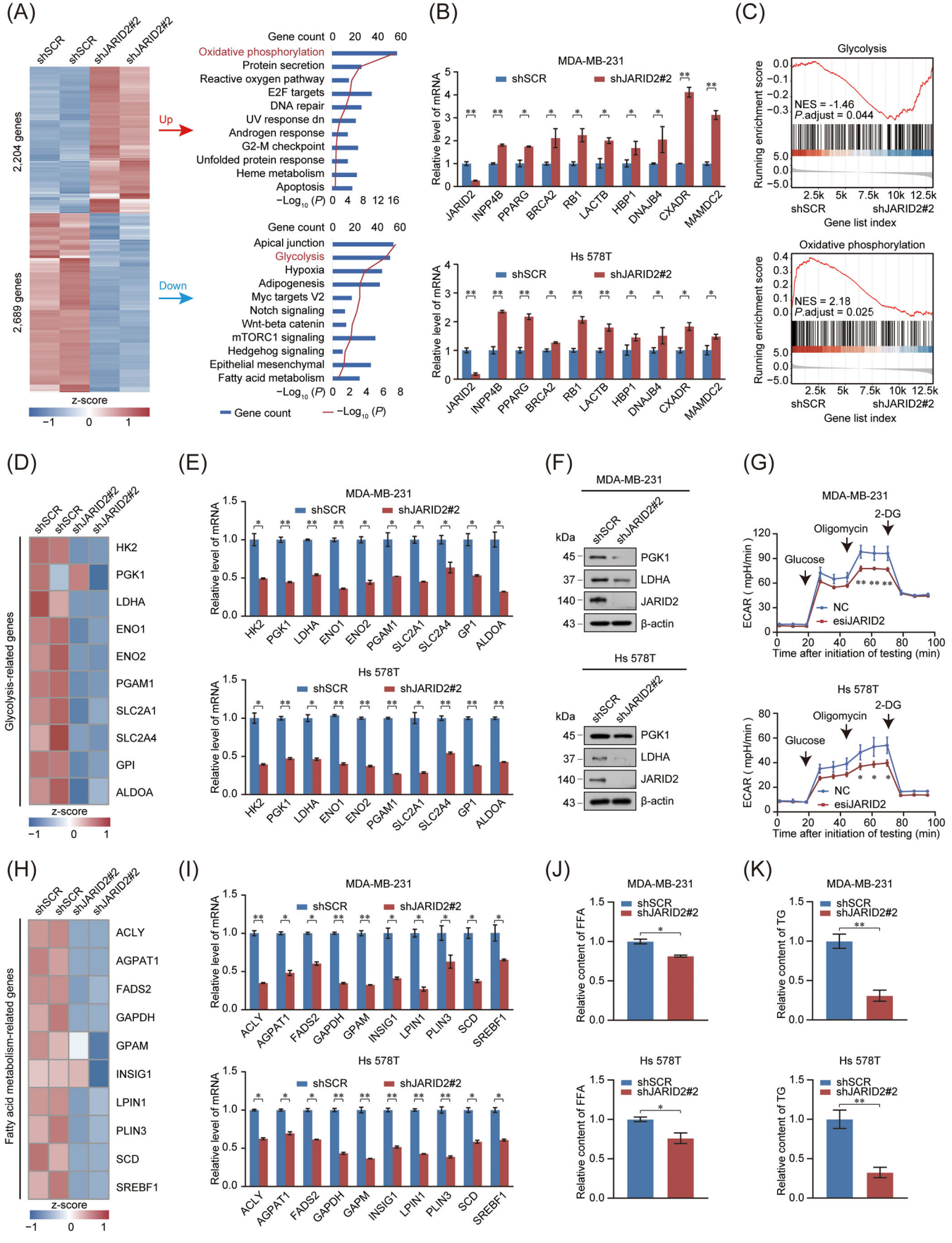
(A)
shSCR
shSCR
shJARID2#2
shJARID2#2
2,204 genes
2,689 genes
Up
Down
z-score
−1
0
1
Gene count 0 20 40 60
Oxidative phosphorylation
Protein secretion
Reactive oxygen pathway
E2F targets
DNA repair
UV response dn
Androgen response
G2-M checkpoint
Unfolded protein response
Heme metabolism
Apoptosis
−Log10 (P) 0 4 8 12 16
Gene count 0 20 40 60
Apical junction
Glycolysis
Hypoxia
Adipogenesis
Myc targets V2
Notch signaling
Wnt-beta catenin
mTORC1 signaling
Hedgehog signaling
Epithelial mesenchymal
Fatty acid metabolism
−Log10 (P) 0 2 4 6 8
Gene count
−Log10 (P)
(B)
MDA-MB-231
shSCR
shJARID2#2
Relative level of mRNA
JARID2
INPP4B
PPARG
BRCA2
RB1
LACTB
HBP1
DNAJB4
CXADR
MAMDC2
Hs 578T
(C)
Glycolysis
NES = -1.46
P.adjust = 0.044
Running enrichment score
2.5k 5k 7.5k 10k 12.5k
shSCR
shJARID2#2
Gene list index
Oxidative phosphorylation
NES = 2.18
P.adjust = 0.025
(D)
Glycolysis-related genes
HK2
PGK1
LDHA
ENO1
ENO2
PGAM1
SLC2A1
SLC2A4
GPI
ALDOA
(E)
(F)
kDa
45
37
140
43
PGK1
LDHA
JARID2
β-actin
(G)
2-DG
Oligomycin
Glucose
ECAR (mpH/min)
NC
esiJARID2
Time after initiation of testing (min)
(H)
Fatty acid metabolism-related genes
ACLY
AGPAT1
FADS2
GAPDH
GPAM
INSIG1
LPIN1
PLIN3
SCD
SREBF1
(I)
(J)
Relative content of FFA
(K)
Relative content of TG

reported PRC2 complex, the components of the NuRD complex [chromodomain helicase DNA-binding protein 4 (CHD4), HDAC2, MTA1, MTA2, and MBD3] were newly identified and co-purified as being associated with the JARID2 protein. All of these associated proteins were also verified via Western blotting (Figure 4A-B). Detailed mass spectrometry data are presented in Supplementary Table S7. To ascertain the intracellular interaction between the NuRD complex and JARID2, co-IP experiment was conducted in MDA-MB-231, Hs 578T, and HEK293T cells, and the experiments demonstrated that JARID2 was physically associated with the NuRD complex (Figure 4C and Supplementary Figure S6). Meanwhile, co-IP of JARID2 with MTA1 was performed in both breast cancer tissues and adjacent normal tissues. The results showed that the interaction between JARID2 and MTA1 was stronger in breast cancer tissues than in adjacent normal tissues (Figure 4D). In summary, our results supported the hypothesis that JARID2 and the NuRD complex functionally cooperated.

As shown in Figure 4E, GST pull-down assays demonstrated that JARID2 directly interacted with MTA1/2 and HDAC1/2. To investigate the detailed mechanism of the interaction between JARID2 and the NuRD complex, JARID2 was truncated and fused with a GST tag (Figure 4F). We found that the L1 domain (1-232 amino acids) of JARID2 mediated the interaction with MTA1/2, and the JmjC domain of JARID2 mediated that with HDAC1/2 (Figure 4G-H). Moreover, the Swi3-Ada2-N-CoR-TFIIIB (SANT) domain of MTA1/2 directly interacted with JARID2, and the N-terminal domain of HDAC1/2 was responsible for this interaction (Figure 4I-J). The GST pull-down experiments further demonstrated that JARID2 and the NuRD complex were physically interrelated. We know that JARID2 is a cofactor of PRC2, and the association between PRC2 and NuRD had been reported and validated [14, 19]. Herein, we also demonstrated that JARID2 interacted with the NuRD complex. Therefore, we intended to explore whether JARID2 was involved in the interaction between PRC2 and the NuRD complex. In the quantitative co-IP experiment, the deletion of JARID2 in MDA-MB-231 and Hs 578T cells disrupted the interaction between the core subunit MTA1 of the NuRD complex and the key component EZH2 of the PRC2 complex (Figure 4K). These results also provided some support for the hypothesis that JARID2 acts as a physical connection between the NuRD and PRC2 complexes. In summary, we provided the molecular details involved in the formation of the JARID2/NuRD complex (Figure 4L).

3.5 | JARID2 and MTA1 collectively promoted breast cancer cell proliferation, invasion, and stemness

Next, we studied the function of the JARID2/NuRD complex in breast cancer cell proliferation, invasion, and stemness. Overexpression of JARID2 or MTA1 significantly enhanced the proliferation of MCF-7 and T-47D cells, whereas knockdown of JARID2 or MTA1 in MDA-MB-231 and Hs 578T cells resulted in the opposite effect. Moreover, the cell number was much higher when JARID2 and MTA1 were both overexpressed in MCF-7 and T-47D cells compared to when only one of them was overexpressed. In MDA-MB-231 and Hs 578T cells, combined knockdown of JARID2 and MTA1 had a greater inhibitory effect on cell proliferation than the knockdown of JARID2 or MTA1 individually (Figure 5A). Colony formation assays

FIGURE 3 JARID2 regulated the expression of TSGs, glycolysis-related genes, and lipid metabolism related genes. (A) Heatmap of expression of differential genes in MDA-MB-231 cells infected with knockdown lentivirus (shSCR, shJARID2#2) is shown. The KEGG pathway of differentially expressed genes is shown on the right. (B) RT-qPCR assays of selected TSGs were conducted in MDA-MB-231 and Hs 578T cells infected with knockdown lentivirus (shSCR, shJARID2#2) for selected TSGs. *ATCB* was used as an internal reference gene. (C) Glycolysis signal pathway (up) and oxidative phosphorylation signal pathway (down) were analyzed by GSEA. (D) Heatmap of glycolysis-related genes selected following RNA-seq. (E) RT-qPCR assays were conducted in MDA-MB-231 and Hs 578T cells infected with knockdown lentivirus (shSCR, shJARID2#2) to evaluate the level of expression of selected glycolysis-related genes. *ATCB* was used as an internal reference gene. (F) Western blotting assays were conducted in MDA-MB-231 and Hs 578T cells infected with knockdown lentivirus (shSCR, shJARID2#2) to detect several glycolysis-related genes. β-actin was used as an internal reference protein. (G) The extracellular acidification rate (ECAR) was measured in breast cancer cells transfected with the indicated JARID2 esiRNA. (H) Heatmap of some lipid metabolism-related genes selected in RNA-seq. (I) RT-qPCR assays were conducted in MDA-MB-231 and Hs 578T cells infected with knockdown lentivirus (shSCR, shJARID2#2) to evaluate the expression of selected lipid metabolism-related genes. *ATCB* was used as an internal reference gene. (J) Relative level of serum-free fatty acid (FFA) was detected in MDA-MB-231 and Hs 578T cells infected with knockdown lentivirus (shSCR, shJARID2#2). (K) Relative level of serum-triglyceride (TG) was detected in MDA-MB-231 and Hs 578T cells infected with knockdown lentivirus (shSCR, shJARID2#2). (B, E, G, I-K) Error bars indicate means ± SD. The data was analyzed by two-tailed unpaired *t*-test, $^{*}P < 0.05$, $^{**}P < 0.01$.

Abbreviations: shSCR, scramble; TSGs, tumor suppressor genes; oe, overexpression; NC, negative control; esiRNA, endoribonuclease-prepared siRNA; KEGG, Kyoto Encyclopedia of Genes and Genomes; GSEA, Gene set enrichment analysis; ECAR, extracellular acidification rate; FFA, free fatty acid; TG, triglyceride.

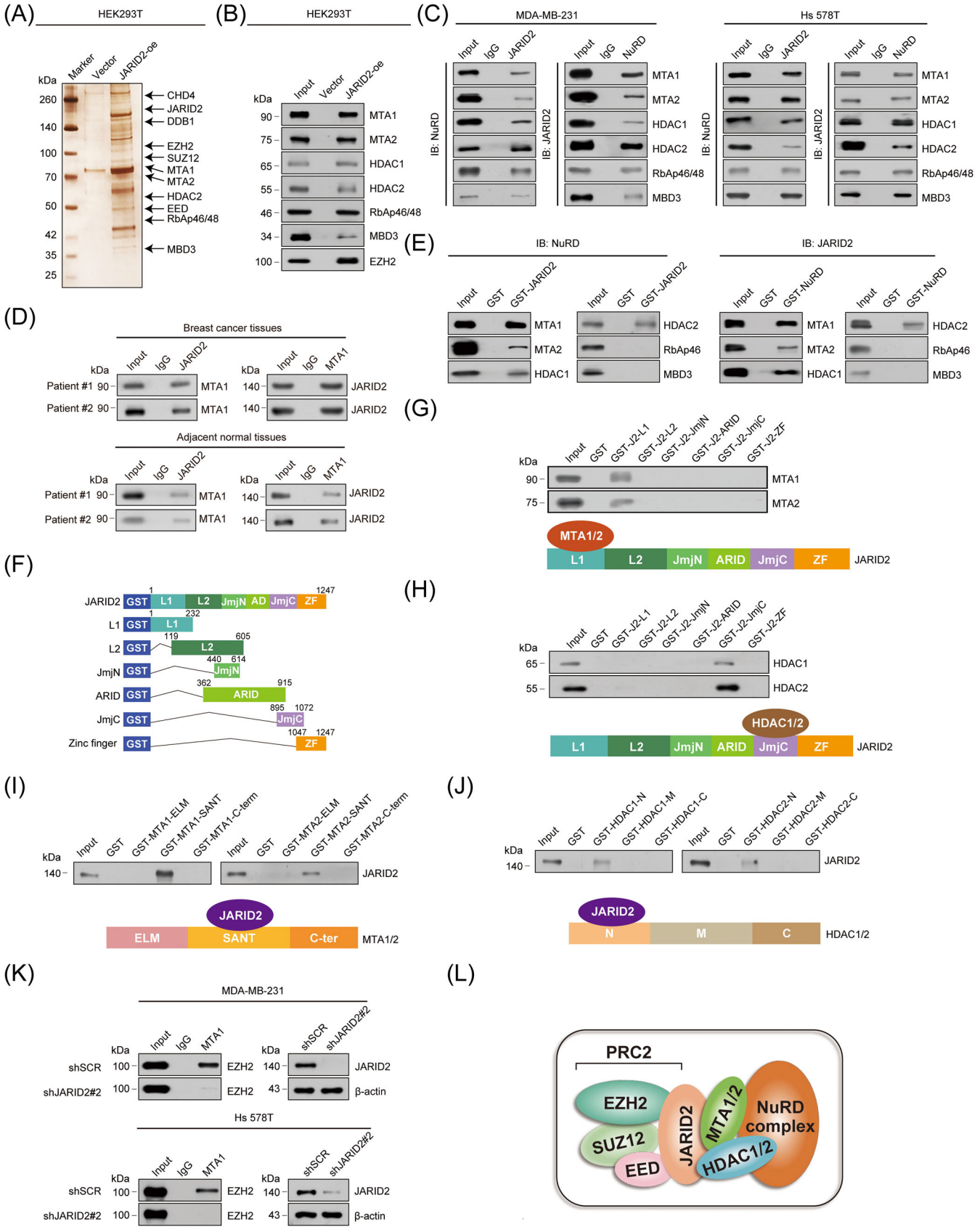

FIGURE 4 Physical association between JARID2 and the NuRD complex. (A-B) HEK293T cells transfected with control vector or FLAG-JARID2 were lysed, anti-FLAG affinity column was used for immunopurification, and FLAG peptide was used for elution. We used mass spectrometry to analyze protein bands that were acquired by dealing with eluent with Nu-PAGE and silver staining. Some binding proteins were verified in HEK293T cells. (C) The lysates of MDA-MB-231 or Hs 578T cells were mixed with anti-JARID2 antibody or antibody

were carried out, and the results showed that the individual JARID2 or MTA1 overexpression was related to an increase in the number of colonies in MCF-7 and T-47D cells, while the overexpression of both JARID2 and MTA1 led to an even higher increase (Figure 5B). Consistently, in MDA-MB-231 and Hs 578T cells, knockdown of JARID2 and MTA1 separately was related to a significant reduction in colony number, and their simultaneous knockdown was related to an even more significant decrease (Figure 5C).

Moreover, we performed transwell invasion assays in MDA-MB-231, Hs 578T, MCF-7, and T-47D breast cancer cells. JARID2 or MTA1 overexpression in MCF-7 and T-47D cells resulted in a conspicuous increase in cell invasion, whereas their knockdown in MDA-MB-231 and Hs 578T cells resulted in a decrease in cell invasion potential. Co-overexpression of JARID2 and MTA1 in MCF-7 and T-47D cells induced a stronger invasive capability. The simultaneous knockdown of JARID2 and MTA1 in MDA-MB-231 and Hs 578T cells led to a significantly lower cell invasion ability compared to the knockdown of only one of them (Figure 5D-E). In addition, JARID2 restored the proliferation and invasion abilities of JARID2-knockdown MDA-MB-231 and Hs 578T cells (Figure 5C and 5E).

Furthermore, we investigated the role of the JARID2/MTA1 complex on the stemness of breast cancer cells using Western blotting (Figure 5F). JARID2 and MTA1 were overexpressed and further knocked down in MDA-MB-231 and T-47D cells, respectively. The Western blotting results showed that the expression of stemness genes was increased when JARID2 or MTA1 was individually overexpressed. In addition, the knockdown of MTA1 in cells stably expressing JARID2 or the knockdown of JARID2 in cells stably expressing MTA1 led to at least a partial decrease in the expression of stemness genes. These results indicated that JARID2 and the MTA1 (NuRD) complex were functionally interdependent and affected the expression of stemness genes.

3.6 | Genome-wide identification of JARID2/NuRD complex transcription targets

To analyze genome-wide JARID2/NuRD complex transcriptional targets, ChIP-seq was conducted using the JARID2 antibody and the published dataset (GSE128231). We found that the enrichment ratio of JARID2 and MTA1 in the promoter region was similar (Supplementary Figure S7A). Meanwhile, we found 10,856 JARID2-specific binding peaks and 10,915 MTA1-specific binding peaks (Supplementary Figure S7B). Next, we found 1,194 JARID2 DNA promoter sequences and 1,090 MTA1 DNA promoter sequences. We overlapped DNA promoter sequences from JARID2 and MTA1 to seek co-targets of the JARID2/NuRD complex. KEGG analysis indicated that these enriched overlapping genes were involved in numerous cellular signaling pathways associated with tumor initiation and progression, including nuclear factor kappa-light-chain-enhancer of activated B cells (NF-κB), mammalian target of rapamycin complex 1 (mTORC1), hypoxia, G2-M checkpoint, fatty acid metabolism, and EMT (Supplementary Figure S7C). Furthermore, qChIP analysis elucidated that JARID2 and MTA1 were enriched in the promoters of selected TSGs, such as *BRCA2*, *RB1*, and *INPP4B* (Supplementary Figure S7D). To determine whether PRC2 was also involved in the regulation of these genes, we detected the enrichment of EZH2 on the promoters of these genes. The experiment showed that EZH2 was significantly enriched in these target genes (Supplementary Figure S7D). qChIP experiments indicated that the recruitment of JARID2, MTA1, and EZH2 to target promoters was reduced in JARID2- and MTA1-knockdown MDA-MB-231 cells (Figure 6A). Therefore, JARID2, NuRD, and PRC2 act as transcriptional repression complexes, mutually advancing the recruitment and stabilization of target gene promoters, thereby restraining gene expression.

The breast cancer susceptibility gene, BRCA2/BRCA1, is relevant for DNA damage repair and is frequently

against the NuRD complex component to perform co-IP with the NuRD complex component or JARID2, respectively. IgG was used as negative control. (D) The lysates of breast cancer tissues or adjacent normal tissues were mixed with anti-JARID2 antibody or antibody against MTA1 to perform co-IP with MTA1 or JARID2, respectively. IgG was used as negative control. (E) We used the combination of GST fusion proteins expressed by bacteria and proteins transcribed/translated in vitro for GST pull-down analysis. (F-H) Segmented GST pull-down analysis was performed using the GST-fused JARID2 L1 domain (L1), L2 domain (L2), JmjN domain (JmjN), ARID domain (ARID), JmjC domain (JmjC) or Zinc Finger domain (ZF), as well as MTA1, MTA2, HDAC1, or HDAC2 transcribed/translated in vitro. (I-J) Segmented GST pull-down analysis was performed using the GST-fused MTA1/2 ELM domain (ELM), SANT domain (SANT), C-ter domain (C-ter), and JARID2 transcribed/translated in vitro; GST-fused HDAC1/2 N domain (N), M domain (M), C domain (C) and JARID2 transcribed/translated in vitro. (K) We used extracts originated from the same amount of MDA-MB-231 or Hs 578T cells infected with knockdown lentivirus (shSCR, shJARID2#2) to perform co-IP assays with MTA1 antibody, and IB with EZH2. (L) The schematic diagram of the molecular interaction among JARID2, NuRD, and PRC2.

Abbreviations: oe, overexpression; SDS-PAGE, sodium dodecyl sulfate polyacrylamide gel electrophoresis; NuRD, nucleosome remodeling and deacetylase; co-IP, co-immunoprecipitation; PRC2, polycomb repressive complex 2.

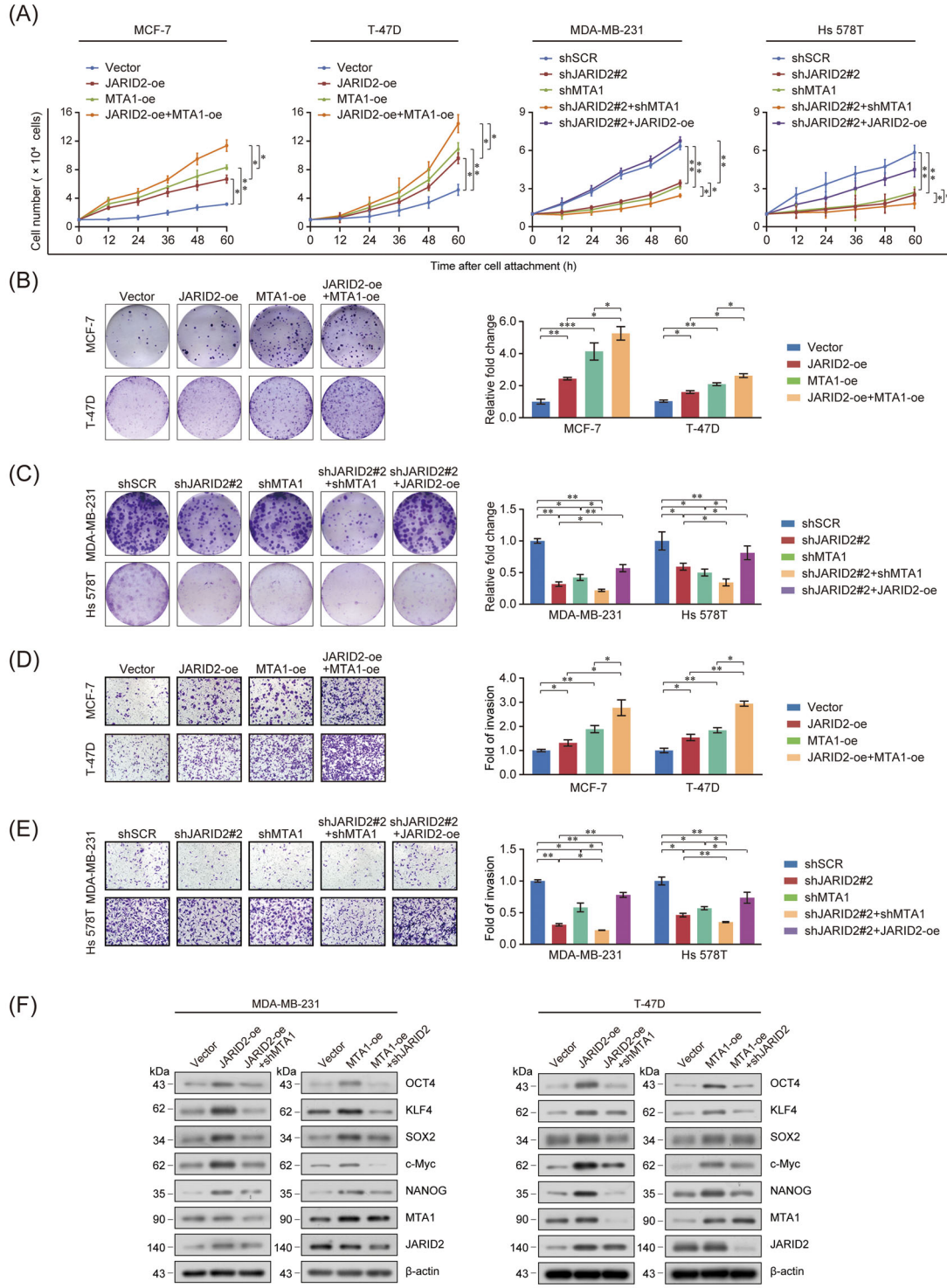

FIGURE 5 JARID2 and MTA1 promoted breast cancer cell proliferation, invasion, and stemness. (A) MCF-7 and T-47D cells were infected with lentivirus containing overexpressed JARID2 or MTA1 (vector, FLAG-JARID2, FLAG-MTA1, and FLAG-JARID2 together with FLAG-MTA1) to perform growth curve analysis. MDA-MB-231 and Hs 578T cells were infected with lentivirus containing knocked down JARID2 or MTA1 (shSCR, shJARID2#2, shMTA1, shJARID2#2 together with shMTA1, and shJARID2#2 with FLAG-JARID2) to perform growth curve analysis. (B-C) Before crystal violet staining, MCF-7, T-47D, MDA-MB-231, and Hs 578T cells treated with the corresponding lentivirus were cultured in the medium for a week. Representative pictures were displayed and analyzed. (D-E) The corresponding lentiviruses were used to transfect MCF-7, T-47D, MDA-MB-231, and Hs 578T cells, and transwell invasion assays were performed. The invading cells were stained with crystal violet and counted by ImageJ. (F) JARID2 or MTA1 was silenced in MDA-MB-231 or T-47D cells stably transfected with vector, MTA1, or JARID2, and the expression of stem cell markers was assessed by Western blotting. β-actin served as a loading control for Western blotting. (A–E) Error bars indicate means ± SD. The data was analyzed by one-way ANOVA, $^{*}P < 0.05$, $^{**}P < 0.01$. Abbreviations: oe, overexpression; shSCR, scramble; esiRNA, endoribonuclease-prepared siRNA.

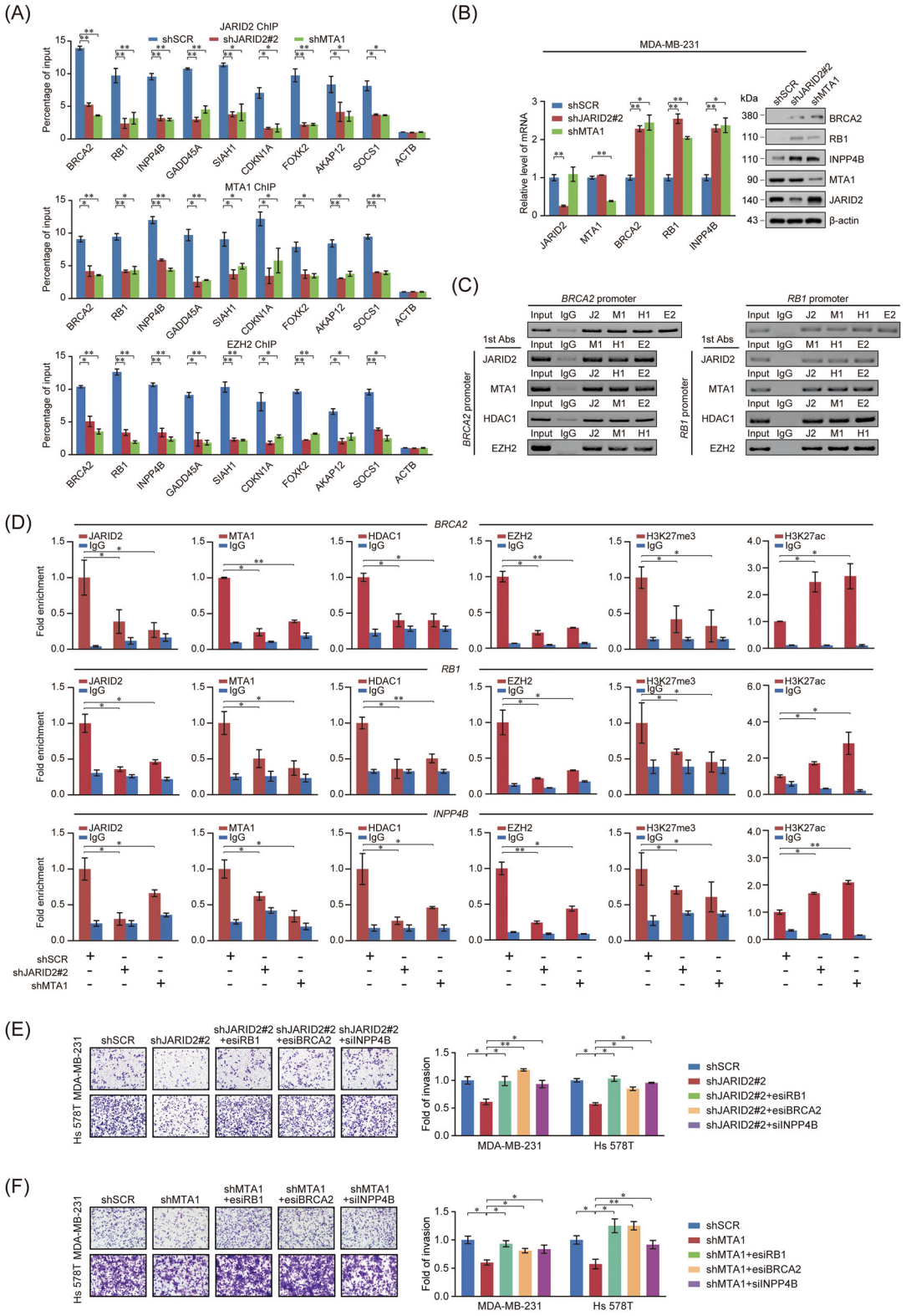

FIGURE 6 Genome-wide identification analyses of transcription targets of the JARID2/NuRD complex in MDA-MB-231 cells. (A) We used antibodies against JARID2, MTA1, or EZH2 in MDA-MB-231 cells infected with knockdown lentivirus (shSCR, shJARID2#2, shMTA1) to perform qChIP analysis for promoters of selected target genes. *ATCB* was used as an internal reference gene. (B) The expression of BRCA2, RB1, and INPP4B was detected in MDA-MB-231 cells infected with knockdown lentiviruses (shSCR, shJARID2#2, shMTA1) by RT-qPCR and Western blotting. *ATCB* was used as an internal reference gene of mRNA level; *β*-actin was used as an internal reference protein for Western blotting. (C) In MDA-MB-231 cells, ChIP/Re-ChIP assays were conducted with the indicated antibodies. J2, JARID2; M1, MTA1; H1, HDAC1; E2, EZH2. (D) The recruitment on *BRCA2*, *RB1*, and *INPP4B* promoters for the indicated proteins was evaluated in MDA-MB-231 cells infected

mutated in breast cancer [33, 34]. RB1 is a well-known transcription inhibitor closely related to the cell cycle [35]. In triple-negative breast cancer, INPP4B has a conspicuous tumor-suppressive effect [36]. Therefore, transcriptional regulation of *BRCA2*, *RB1*, and *INPP4B* by the JARID2/NuRD complex was investigated. JARID2 or MTA1 knockdown increased the mRNA and protein expression of *BRCA2*, *RB1*, and *INPP4B* in MDA-MB-231 and Hs 578T cells (Figure 6B and Supplementary Figure S7E). JARID2 acts as a bridge between the NuRD and PRC2 complex. Furthermore, we found that the PRC2 core subunit EZH2 regulated downstream target genes, along with the JARID2/NuRD complex (Figure 6C and Supplementary Figure S7F). Moreover, qChIP analyses indicated that JARID2 or MTA1 knockdown led to a remarkable decrease in the recruitment of JARID2, MTA1, HDAC1, and EZH2 to *BRCA2*, *RB1*, and *INPP4B* promoters. Notably, JARID2 or MTA1 knockdown resulted in decreased H3K27me3 levels and increased H3K27ac levels at the *BRCA2*, *RB1*, and *INPP4B* promoters (Figure 6D), which indirectly indicated that the binding between the JARID2/NuRD complex and *BRCA2*, *RB1*, and *INPP4B* promoters was dependent on PRC2, accompanied by demethylation and deacetylation of histones. Meanwhile, a JARID2-high breast cancer tissue and a JARID2-low breast cancer tissue were selected and confirmed by Western blotting (Supplementary Figure S7G). ChIP-qPCR experiments demonstrated that the H3K27me3 enrichments at *RB1*, *BRCA2*, and *INPP4B* promoters were higher in the JARID2-high breast cancer tissue compared to the JARID2-low breast cancer tissue; the opposite phenomenon was observed for H3K27ac (Supplementary Figure S7H-I).

In conclusion, these experiments further confirmed that the JARID2/NuRD/PRC2 complex was functionally linked to the synergistic transcriptional repression of a series of target genes, like *BRCA2*, *RB1*, and *INPP4B*. Furthermore, JARID2 or MTA1 knockdown in MDA-MB-231 and Hs 578T cells reduced the cell invasion potential, partially reversed by co-knockdown of *BRCA2*, *RB1*, or *INPP4B* using esi- or siRNAs (Figure 6E-F and Supplementary Figure S8). These results supported that the JARID2/MTA1 complex promoted the invasive potential of breast cancer cells, partially by repressing *BRCA2*, *RB1*, and *INPP4B*.

3.7 | JARID2 expression was upregulated in breast cancer cells by adipocyte-derived leptin through the JAK2/STAT3 pathway

Recently, metabolic reprogramming has been defined as one of the top ten hallmarks of cancer [37]. Furthermore, obesity is a risk factor for postmenopausal breast cancer [24]. Herein, we demonstrated that JARID2 was involved in changes in several metabolic pathways (Figure 3A). Therefore, we investigated whether the abundant number of adipocytes in the tumor microenvironment influences the expression of JARID2 in breast cancer cells. First, we established a coculture system of breast cancer cells and adipocytes (Figure 7A). Then, Oil Red O staining and detection of the expression of peroxisome proliferator-activated receptor γ (PPARγ) were performed to confirm the differentiation of preadipocytes into mature adipocytes (Supplementary Figure S9A). The results showed that the invasion capability of MDA-MB-231 and Hs 578T cells was enhanced when cocultured with adipocytes compared with that of tumor cells alone (Figure 7B). Interestingly, the expression of JARID2 was upregulated when breast cancer cells were cocultured with adipocytes (Figure 7C). However, the enhanced invasion ability of MDA-MB-231 and Hs 578T cells stimulated by adipocytes was abolished when JARID2 was knocked down (Figure 7D). We performed the same experiments in MCF-7 and T-47D cells and obtained similar results (Supplementary Figure S9B-D). In addition, we detected the changes in the level of expression of some cytokines secreted by adipocytes after coculturing MDA-MB-231 cells with adipocytes. The results showed that the transcription level of leptin was the most significantly altered cytokine in adipocytes (Supplementary Figure S9E). Furthermore, we found that siRNA-targeting LEPR blocked the upregulation of the expression of JARID2 induced by the coculture of breast cancer cells with adipocytes (Supplementary Figure S9F-G), further supporting the role of leptin in regulating the expression of JARID2. Therefore, our subsequent experiments focused on the effects of leptin on breast cancer cells. Adipocyte-derived leptin promotes a range of phenotypic features of breast cancer cells, such as their proliferation and invasion [38]. In this study, we treated MDA-MB-231 cells with leptin at different concentrations and different time inter-

with knockdown lentiviruses (shSCR, shJARID2#2, shMTA1) by qChIP analysis. Purified rabbit IgG was used as an internal reference control. (E-F) The corresponding lentiviruses or those combined with esiBRCA2, esiRB1, or siINPP4B, were used to transfect MDA-MB-231 and Hs 578T cells and to perform transwell invasion assays. The invading cells were stained with crystal violet and counted using ImageJ. (A–B, D) Error bars indicate means ± SD. The data was analyzed by two-tailed unpaired *t*-test and one-way ANOVA (E–F), $^{*}P < 0.05$, $^{**}P < 0.01$. Abbreviations: ChIP, Chromatin immunoprecipitation; qChIP, quantitative ChIP; shSCR, scramble; esiRNA, endoribonuclease-prepared siRNA; BRCA2, BRCA2 DNA repair associated; RB1, RB transcriptional corepressor 1; INPP4B, inositol polyphosphate-4-phosphatase type II B.

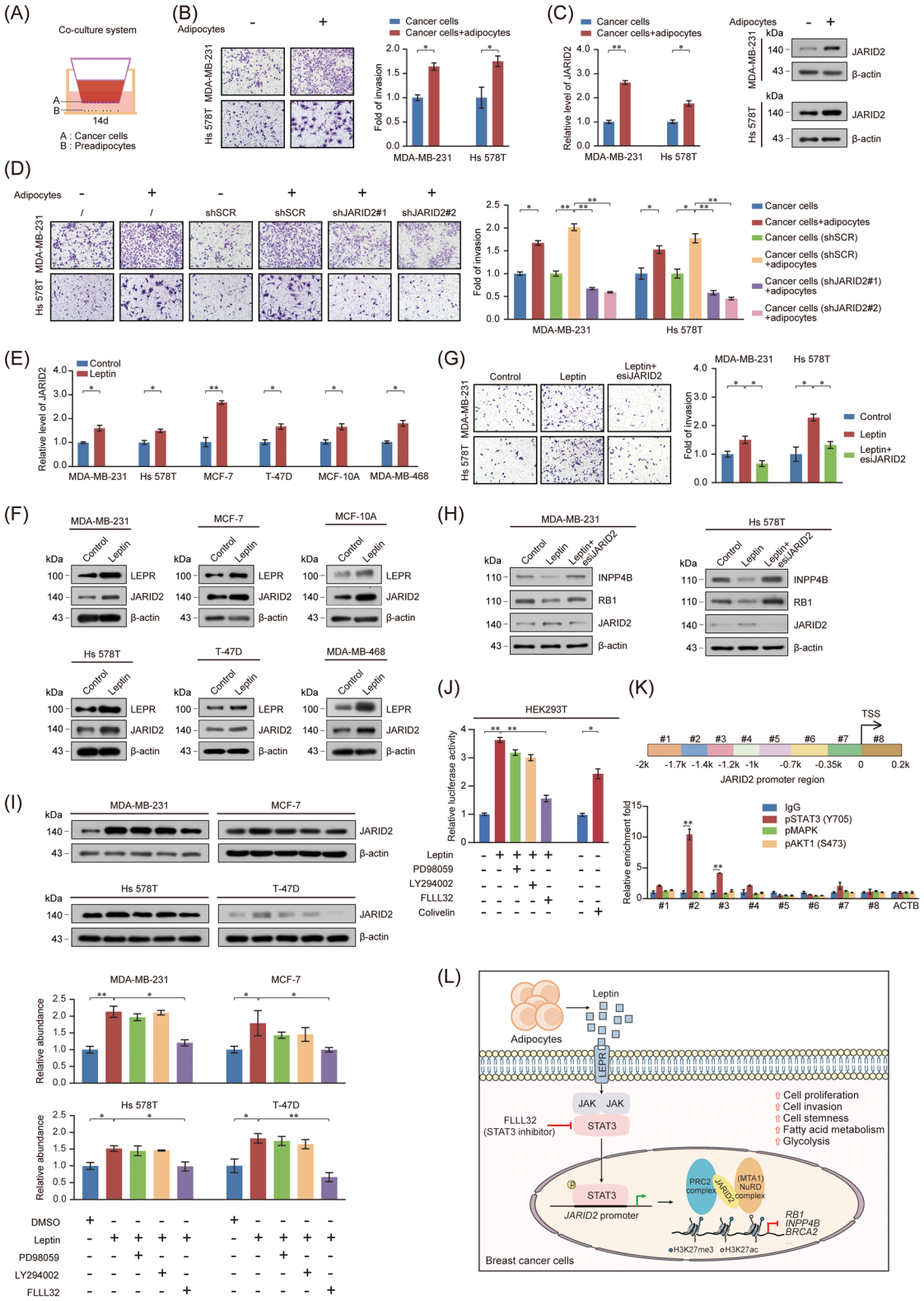

FIGURE 7 JARID2 expression was upregulated by adipocyte-derived leptin through the JAK2/STAT3 pathway in breast cancer cells. (A) Schematic diagram of the breast cancer cells (bottom layer) and adipocytes (upper layer) coculture system. Cells were then cocultured for three days. (B) MDA-MB-231 or Hs 578T cells were cocultured with or without adipocytes for three days. Then, cancer cells were harvested to perform invasion assays. (C) The JARID2 expression was detected by RT-qPCR and Western blotting in MDA-MB-231 or Hs 578T cells cocultured with or without adipocytes. (D) MDA-MB-231 and Hs 578T cells with JARID2 knockdown or not, were cocultured with or without adipocytes. The cancer cells were harvested to conduct invasion assays. (E-F) The mRNA and protein levels of JARID2 were detected by RT-qPCR and Western blotting in MDA-MB-231, Hs 578T, MCF-7, and T-47D cells that were treated with leptin. (G) MDA-MB-231 and Hs 578T cells were transfected with the indicated siRNAs and then treated with leptin. The cells were used to conduct transwell assays. (H)

vals to identify appropriate treatment concentration and duration of exposure. We found that leptin led to elevated JARID2 expression at 150 ng/mL and after 24 h of exposure (Supplementary Figure S9H). Similarly, JARID2 expression was increased under stimulation with exogenous leptin in normal breast epithelial cells and various breast cancer cell lines (Figure 7E-F). Moreover, exogenous leptin remarkably promoted invasion ability of MDA-MB-231 and Hs 578T cells, whereas JARID2 knockdown abrogated this effect (Figure 7G). Furthermore, INPP4B and RB1 protein levels were inhibited by leptin treatment, while JARID2 knockdown restored their expression (Figure 7H). Considering these results, we concluded that leptin derived from adipocytes induced the upregulation of JARID2 expression and promoted the invasion of breast cancer cells.

Leptin binds to LEPR on cell surface and subsequently regulates various signaling cascades, including PI3K/AKT, JAK2/STAT3, and MAPK/ERK. In cancer, all of these pathways are often dysregulated [39]. Using Western blotting, we examined whether FLLL32 (a JAK2/STAT3 inhibitor), LY294002 (a PI3K/AKT inhibitor), or PD98059 (a MAPK/ERK inhibitor) influence the elevated JARID2 expression in leptin-treated breast cancer cells. The results indicated that FLLL32 blocked the leptin-induced upregulation of JARID2 expression (Figure 7I and Supplementary Figure S9I), implying that the JAK2/STAT3 signaling pathway was involved in regulating leptin-mediated JARID2 expression. The analysis of ENCODE Transcription Factor Target, hTFtarget, CHEA Transcription Factor Target, and JASPAR Predicted Transcription databases also showed that JARID2 was the target gene of STAT3 (Supplementary Figure S9J). Motif analysis also yielded a similar result (Supplementary Figure S9K). The pGL3 vector containing the JARID2 promoter and the substrate were co-transfected into HEK293T cells to further explore this interaction. Luciferase reporter gene experiments revealed that FLLL32 inhibited the activation of JARID2 promoter, whereas the other two inhibitors (PD98509 and LY294002) had little effect (Figure 7J). Furthermore, qChIP experiments showed that p-STAT3 could directly bind to the promoter and regulate the activation of JARID2 expression, while the antibodies interfering with the other two pathways had little effect (Figure 7K). Meanwhile, we designed experiments to verify whether the inhibition of the JAK2/STAT3 pathway affected the interaction of JARID2 with the NuRD complex. The results of quantitative co-IP experiments showed that the inhibition of the JAK2/STAT3 pathway by FLLL32 determined the disruption of the interaction between JARID2 and the NuRD complex (Supplementary Figure S9L). Considering these results, we performed ChIP-qPCR experiments to examine the enrichment of H3K27me3 and H3K27ac at *RB1*, *BRCA2*, and *INPP4B* promoters in MDA-MB-231 cells treated with DMSO or FLLL32. The results indicated that FLLL32 reduced the H3K27me3 enrichment and increased the H3K27ac enrichment at *RB1*, *BRCA2*, and *INPP4B* promoters compared to DMSO (Supplementary Figure S9M). Based on these results, we concluded that adipocyte-derived leptin increased the expression of JARID2 through the JAK2/STAT3 pathway, thereby influencing the invasive ability of breast cancer cells (Figure 7L).

3.8 | JARID2 expression was upregulated in a variety of cancers

Finally, to understand the connection between JARID2 and the clinicopathological data, we analyzed the expression of JARID2 and the clinical outcome of the corresponding patients with breast cancer. Published clinical datasets (GSE9195 and GSE58812) were analyzed using Kaplan-Meier curves, and the results indicated that the expression of *JARID2* and *MTA1* were relevant to OS, RFS, MFS, and DMFS in patients with breast cancer (Figure 8A). To ascertain the function of JARID2 in other types of tumors, a range of tumor samples from

MDA-MB-231 and Hs 578T cells were transfected with indicated siRNAs and further treated with leptin. The levels of JARID2, RB1, and INPP4B were detected by Western blotting. β-actin served as a loading control. (I) Serum-starved MDA-MB-231, Hs 578T, MCF-7, or T-47D cells were pre-treated with DMSO, PD980590 (ERK inhibitor, 10 μmol/L), LY294002 (PI3K inhibitor, 20 μmol/L), or FLLL32 (JAK inhibitor, 50 μmol/L) for 1 h and further treated with leptin (150 ng/mL) for 48 h. JARID2 expression was detected by Western blotting. (J) HEK293T cells were transfected with indicated plasmid and further treated with leptin, FLLL32, or Colivelin (STAT3 activator) for 24 h. The luciferase levels were measured. (K) The ChIP experiment was conducted using IgG, pSTAT3(Y705), pMAPK, and pAKT1(S473) antibodies in MDA-MB-231 cells. The STAT3 binding region of *JARID2* promoter was detected by qChIP. The results were normalized to input DNA. (L) Schematic representation of the molecular interaction between leptin/JARID2/NuRD and PRC2 complexes. Adipocyte-derived leptin activates JARID2 expression via JAK2/STAT3 signaling pathway. JARID2 combines with NuRD and PRC2 complexes to promote the proliferation, invasion, stemness, glycolysis, and fatty acid metabolism in breast cancer. (B-D, E-G, J, K) Error bars indicate means ± SD. The data were analyzed by one-way ANOVA (D, G, J) or two-tailed unpaired *t*-test (B-C, E-F, K), $^*P < 0.05$, $^{**}P < 0.01$.

Abbreviations: shSCR, scramble; esiRNA, endoribonuclease-prepared siRNA; TSS, transcription start site; RT-qPCR, real-time quantitative PCR; qChIP, quantitative ChIP; NuRD, nucleosome remodeling and deacetylase; PRC2, polycomb repressive complex 2; JAK2/STAT3, Janus kinase/signal transducer and activator of transcription 3.

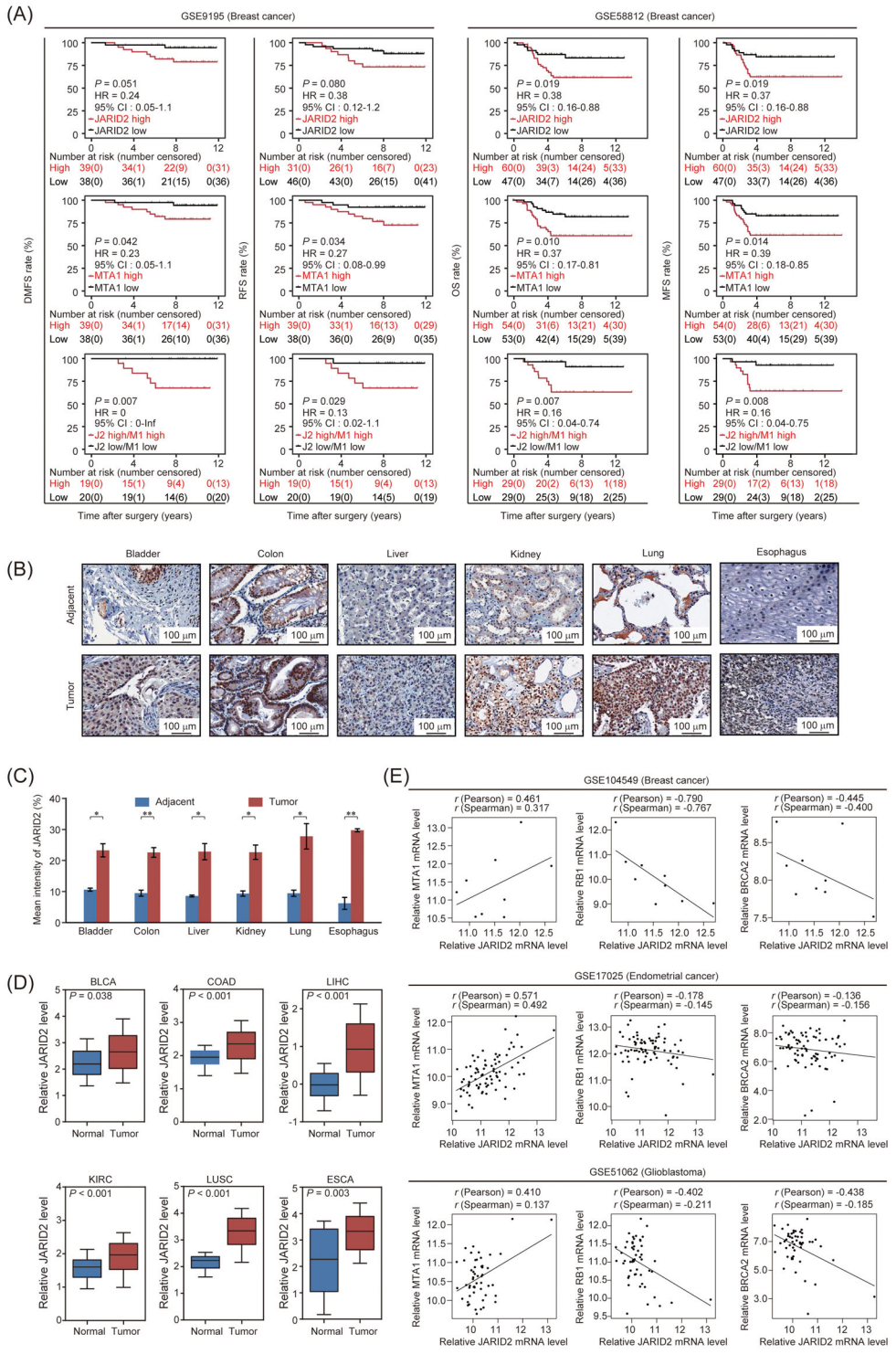

FIGURE 8 JARID2 expression was upregulated in a variety of cancers. (A) The relationship between *JARID2*, *MTA1* expression and survival time was analyzed by Kaplan-Meier survival analysis using GSE9195 or GSE58812 datasets. (B-C) In normal tissue and the corresponding tumor tissue of the bladder, colon, liver, kidney, lung, and esophagus, the immunohistochemical staining of JARID2 expression was analyzed using IHC staining. (D) JARID2 expression in the datasets available from TCGA. (E) The published clinical datasets (GSE104549, GSE17025, and GSE51062) were analyzed to understand the relationship between the expression of *MTA1*, *RB1*, *BRCA2,* and *JARID2*. (C-E) Error bars indicate means ± SD. The data was analyzed by two-tailed unpaired *t*-test, $^{*}P < 0.05$, $^{**}P < 0.01$.
Abbreviations: HR, hazard ratio; IHC, immunohistochemical; TCGA, The Cancer Genome Atlas; GEO, Gene Expression Omnibus; COAD, Colon adenocarcinoma; BLCA, Bladder urothelial carcinoma; KIRC, Kidney renal clear cell carcinoma; LUSC, Lung squamous cell carcinoma; LIHC, Liver hepatocellular carcinoma; ESCA, Esophageal carcinoma; DMFS, distant metastasis-free survival; RFS, relapse-free survival; OS, overall survival; MFS, metastasis-free survival.

patients were collected. Significantly upregulated expression of JARID2 was observed by IHC staining in several tumors including bladder, colon, liver, kidney, lung, and esophageal cancers (Figure 8B-C). In addition, analysis of the TCGA database demonstrated that the expression of JARID2 was higher in multiple types of cancer tissues than in adjacent normal tissues (Figure 8D). Analysis of several published clinical datasets (GSE104549, GSE17025, and GSE51062) revealed that *MTA1* expression was positively correlated with *JARID2* expression, while *BRCA2* and *RB1* expressions were negatively correlated with the *JARID2* expression (Figure 8E). In conclusion, our results showed that JARID2 was upregulated in various cancers. Thus, it can be a potential cancer biomarker and therapeutic target.

4 | DISCUSSION

Our results showed that the expression of JARID2 was upregulated in breast cancer cells by adipocyte-secreted leptin via the JAK2/STAT3 pathway. JARID2, physically associated with the NuRD complex, silenced several TSGs, such as *BRCA2*, *RB1*, and *INPP4B*, at transcriptional level and enhanced stemness, glycolysis, lipid metabolism, proliferation, and invasiveness of breast cancer cells. Furthermore, the expression of JARID2 was conspicuously upregulated in various types of human cancers and was associated with poor prognosis of breast cancer, implying that JARID2 can be regarded as a potential therapeutic target for the treatment of cancer.

JARID2 is an important oncoprotein and is associated with cancer metastasis [40]. It enhances bladder cancer progression by regulating phosphatase and tensin homolog deleted on chromosome 10/protein kinase B (PTEN/AKT) signaling [41]. Similarly, JARID2 and the PRC2 complexes also regulate the skeletal muscle cell cycle [42]. In the present study, analysis of the TCGA database confirmed that upregulation of JARID2 expression was detected in several malignancies, including breast cancer. The increased expression of JARID2 was found in multiple GEO databases. We also found that the joint high expression of JARID2 and MTA1 was associated with a decrease in OS, RFS, MFS, and DMFS of patients with breast cancer. JARID2 knockdown was accompanied by the upregulation of some TSGs. These results demonstrated that JARID2 is a potential cancer biomarker.

The NuRD complex-induced deacetylation and PRC2-mediated methylation were indirectly relevant and inhibited gene expression [15]. Using mass spectrometry analysis, we confirmed that JARID2 recruited the NuRD complex to form a transcriptional inhibitory unit. The complex inhibited the expression of various TSGs, including *BRCA2*, *RB1*, and *INPP4B*. Furthermore, JARID2, which interacted with the NuRD complex, promoted the proliferation and invasiveness of breast cancer cells. Interestingly, in the absence of JARID2, the crosstalk between the NuRD (MTA1) and PRC2 (EZH2) complexes was remarkably weakened, leading to the attenuation of the transcriptional inhibitory activity of downstream target genes.

CSCs have been identified as a class of cancer cells capable of initiating tumors, maintaining tumors, and regenerating and have emerged as a pathogenic factor in cancer [43]. Accumulating evidence suggests that in many types of cancer, CSCs could drive tumorigenesis, tumor invasion, and metastasis as well as enhanced resistance to radiotherapy and chemotherapy [44, 45]. In the present study, we found that JARID2 was positively related to stemness maintenance of breast cancer cells, indicating that JARID2 is a regulator of CSCs contributing to therapy resistance. NOD/SCID mouse xenograft experiments also revealed that JARID2 knockdown remarkably inhibited tumor growth, tumor-initiating capability, and CSC frequency, further supporting its function as a regulator of breast CSCs. In addition, a previous study indicated that JARID2 was essential for differentiation [9], thus providing an alternative perspective for JARID2's role in breast cancer. Similarly, JARID2 promoted stemness and cisplatin resistance through upregulation of the NOTCH1 pathway in non-small cell lung cancer [46].

Our experimental results also revealed that JARID2 knockdown reduced the glycolytic capacity and influenced the survival and invasion of breast cancer cells. The results also showed that the knockdown of JARID2 disrupted lipid metabolism in tumor cells. Tumor cells utilize glycolysis and lipid metabolism to provide energy for their survival, development, proliferation, and invasion. The level of lipid metabolism varies according to the development of different tumors, and its abnormal variation has a guiding significance for disease determination and prognosis [47]. Our experimental results demonstrated that overexpression of JARID2 in breast cancer resulted in increased tumor proliferation and invasion potential, which might be caused by the promotion of glycolysis and lipid metabolism.

According to previous studies, leptin secreted by adipocytes could promote the proliferation and invasiveness of cancer cells [48, 49]. In the present study, we demonstrated that leptin secreted by adipocytes directly regulated JARID2 expression through the JAK2/STAT3 pathway, influencing the growth and invasion of breast cancer cells. Furthermore, one study revealed that the leptin-LEPR-JAK-STAT3-FAO axis was vital for the self-renewal of breast CSCs [50], which is partly supported by our findings. Furthermore, the increase in fatty acids observed in obesity was related to the inhibition of

glycolysis in $CD8^+$ T cells, limiting the antitumor function of $CD8^+$ T cells via the leptin/PD-1-STAT3-FAO pathway [51]. Considering the herein described influence of adipocytes on breast cancer, we also consider increasing physical exercise to prevent obesity and using diet pills together with anti-cancer drugs, as future tools for fighting cancer.

In the present study, we demonstrated that adipocytes promoted the invasion of breast cancer cells by upregulating the expression of JARID2 in breast cancer cells. However, we have not done corresponding research on the interaction between breast cancer and other types of cells such as immune cells in the tumor microenvironment. We found no drugs targeting JARID2 to improve our research. Our research results were partly based on the fact that breast cancer has a relatively high fat content. We have not studied whether leptin plays a similar role in cancer with low fat content, such as lung cancer. In the present study, we proved that leptin could regulate the expression of JARID2 in breast cancer cells, thus affecting their phenotypes. However, the specific regulatory effect of other adipokines on breast cancer requires further analysis.

5 | CONCLUSIONS

In conclusion, we found that JARID2 expression is directly regulated by adipocyte-derived leptin. Mechanistically, JARID2 physically interacts with the NuRD complex and regulates the expression of glycolysis-related genes, lipid metabolism-related genes, and TSGs, thus contributing to cancer cell proliferation and invasion and enhancing glycolysis and lipid metabolism. Additionally, JARID2 is highly expressed in multiple types of cancer and is associated with poor breast cancer prognosis and with the enhancement of breast cancer cell stemness, suggesting that it is a potential therapeutic target against breast cancer.

DECLARATIONS

AUTHOR CONTRIBUTIONS

WH, YKY and YW supervised the project; WL, YZ, WH, YKY and YW conceived and designed the study; WL and YZ performed experiments and generated figures; XW and JXL provided the clinical samples; XHH, TYG, MDW, JYZ, MMH, TH, TYM, DZ, XT, HFY, MZ and BWY participated in experiments and data analysis. WL and YZ wrote the manuscript. WH, YKY and YW revised the manuscript.

ACKNOWLEDGEMENTS

The authors have nothing to report.

CONFLICTS OF INTEREST STATEMENT

The authors declare that they have no competing interests.

FUNDING INFORMATION

This work was supported by grants from the National Natural Science Foundation of China (41931291, 42125707, 82273403, 82203820, and 82002993), Major State Basic Research Development Program of China (2022YFA1103402), the Non-profit Central Research Institute Fund of Chinese Academy of Medical Sciences (2019PT310027, 2021-RC310-006), the Chinese Academy of Medical Sciences Innovation Fund for Medical Sciences (2021-I2M-1-018), and China Postdoctoral Science Foundation (2022M710454).

ETHICS APPROVAL AND CONSENT TO PARTICIPATE

The 6 paired human tissues were collected using protocols authorized by the Ethics Committee of Cancer Hospital, Chinese Academy of Medical Sciences (permit number: 22/393-3595), and informed consent was acquired from all patients. Animal handling and procedures were approved by Tianjin Medical University Institutional Animal Care Center (permit number: SYXK2019-0001).

CONSENT FOR PUBLICATION

Not applicable.

DATA AVAILABILITY STATEMENT

Raw data for the RNA-seq and ChIP-seq results in this study are uploaded to Gene Expression Omnibus (GEO): GSE202868, GSE202867, respectively.

ORCID

Xin Wang https://orcid.org/0000-0003-1753-2786
Yunkai Yang https://orcid.org/0000-0002-7034-5077
Yan Wang https://orcid.org/0000-0003-2563-255X

REFERENCES

1. Sung H, Ferlay J, Siegel RL, Laversanne M, Soerjomataram I, Jemal A et al. Global cancer statistics 2020: GLOBOCAN estimates of incidence and mortality worldwide for 36 cancers in 185 countries. CA Cancer J Clin. 2021;71(3):209–49.
2. Hong R, Xu B. Breast cancer: an up-to-date review and future perspectives. Cancer Commun (Lond). 2022;42(10):913–36.
3. Britt KL, Cuzick J, Phillips KA. Key steps for effective breast cancer prevention. Nat Rev Cancer. 2020;20(8):417–36.
4. Lei S, Zheng R, Zhang S, Wang S, Chen R, Sun K, et al. Global patterns of breast cancer incidence and mortality: A population-based cancer registry data analysis from 2000 to 2020. Cancer Commun (Lond). 2021;41(11):1183–94.
5. Klose RJ, Kallin EM, Zhang Y. JmjC-domain-containing proteins and histone demethylation. Nature Reviews Genetics. 2006 2006/09/01;7(9):715–27.

6. Landeira D, Fisher AG. Inactive yet indispensable: the tale of Jarid2. Trends Cell Biol. 2011;21(2):74–80.
7. Shen X, Kim W, Fujiwara Y, Simon MD, Liu Y, Mysliwiec MR, et al. Jumonji modulates polycomb activity and self-renewal versus differentiation of stem cells. Cell. 2009;139(7):1303–14.
8. Peng JC, Valouev A, Swigut T, Zhang J, Zhao Y, Sidow A, et al. Jarid2/Jumonji coordinates control of PRC2 enzymatic activity and target gene occupancy in pluripotent cells. Cell. 2009;139(7):1290–302.
9. Landeira D, Sauer S, Poot R, Dvorkina M, Mazzarella L, Jorgensen HF, et al. Jarid2 is a PRC2 component in embryonic stem cells required for multi-lineage differentiation and recruitment of PRC1 and RNA Polymerase II to developmental regulators. Nat Cell Biol. 2010;12(6):618–24.
10. Cooper S, Grijzenhout A, Underwood E, Ancelin K, Zhang T, Nesterova TB,et al. Jarid2 binds mono-ubiquitylated H2A lysine 119 to mediate crosstalk between Polycomb complexes PRC1 and PRC2. Nat Commun. 2016;7:13661.
11. Kasinath V, Beck C, Sauer P, Poepsel S, Kosmatka J, Faini M, et al. JARID2 and AEBP2 regulate PRC2 in the presence of H2AK119ub1 and other histone modifications. Science. 2021;371(6527).
12. Sanulli S, Justin N, Teissandier A, Ancelin K, Portoso M, Caron M, et al. Jarid2 methylation via the PRC2 complex regulates H3K27me3 deposition during cell differentiation. Mol Cell. 2015;57(5):769–83.
13. Kasinath V, Faini M, Poepsel S, Reif D, Feng XA, Stjepanovic G, et al. Structures of human PRC2 with its cofactors AEBP2 and JARID2. Science. 2018;359(6378):940–44.
14. Laugesen A, Helin K. Chromatin repressive complexes in stem cells, development, and cancer. Cell Stem Cell. 2014;14(6):735–51.
15. Torchy MP, Hamiche A, Klaholz BP. Structure and function insights into the NuRD chromatin remodeling complex. Cell Mol Life Sci. 2015;72(13):2491–507.
16. Lai AY, Wade PA. Cancer biology and NuRD: a multifaceted chromatin remodelling complex. Nat Rev Cancer. 2011;11(8):588–96.
17. Xia L, Huang W, Bellani M, Seidman MM, Wu K, Fan D, et al. CHD4 has oncogenic functions in initiating and maintaining epigenetic suppression of multiple tumor suppressor genes. Cancer Cell. 2017;31(5):653–68 e7.
18. Nair SS, Li DQ, Kumar R. A core chromatin remodeling factor instructs global chromatin signaling through multivalent reading of nucleosome codes. Mol Cell. 2013;49(4):704–18.
19. Reynolds N, Salmon-Divon M, Dvinge H, Hynes-Allen A, Balasooriya G, Leaford D, et al. NuRD-mediated deacetylation of H3K27 facilitates recruitment of Polycomb Repressive Complex 2 to direct gene repression. Embo j. 2012;31(3):593–605.
20. Hou Y, Liu W, Yi X, Yang Y, Su D, Huang W, et al. PHF20L1 as a H3K27me2 reader coordinates with transcriptional repressors to promote breast tumorigenesis. Sci Adv. 2020;6(16):eaaz0356.
21. Vander Heiden MG, Cantley LC, Thompson CB. Understanding the Warburg effect: the metabolic requirements of cell proliferation. Science. 2009;324(5930):1029–33.
22. Lunt SY, Vander Heiden MG. Aerobic glycolysis: meeting the metabolic requirements of cell proliferation. Annu Rev Cell Dev Biol. 2011;27:441–64.
23. Yin X, Chen Y, Ruze R, Xu R, Song J, Wang C, et al. The evolving view of thermogenic fat and its implications in cancer and metabolic diseases. Signal Transduct Target Ther. 2022;7(1):324.
24. Soerjomataram I, Bray F. Planning for tomorrow: global cancer incidence and the role of prevention 2020-2070. Nat Rev Clin Oncol. 2021;18(10):663–72.
25. Barone I, Giordano C, Bonofiglio D, Andò S, Catalano S. The weight of obesity in breast cancer progression and metastasis: Clinical and molecular perspectives. Semin Cancer Biol. 2020;60:274–84.
26. Brown KA. Metabolic pathways in obesity-related breast cancer. Nat Rev Endocrinol. 2021;17(6):350–63.
27. Huang W, Zhang J, Huo M, Gao J, Yang T, Yin X, et al. CUL4B Promotes Breast Carcinogenesis by Coordinating with Transcriptional Repressor Complexes in Response to Hypoxia Signaling Pathway. Adv Sci (Weinh). 2021;8(10):2001515.
28. Hu Y, Smyth GK. ELDA: extreme limiting dilution analysis for comparing depleted and enriched populations in stem cell and other assays. J Immunol Methods. 2009;347(1-2):70–8.
29. Gao L, Wu ZX, Assaraf YG, Chen ZS, Wang L. Overcoming anticancer drug resistance via restoration of tumor suppressor gene function. Drug Resist Updat. 2021;57:100770.
30. Chen L, Liu S, Tao Y. Regulating tumor suppressor genes: post-translational modifications. Signal Transduct Target Ther. 2020;5(1):90.
31. Schwartz L, Supuran CT, Alfarouk KO. The Warburg Effect and the Hallmarks of Cancer. Anticancer Agents Med Chem. 2017;17(2):164–70.
32. Pasini D, Cloos PA, Walfridsson J, Olsson L, Bukowski JP, Johansen JV, et al. JARID2 regulates binding of the Polycomb repressive complex 2 to target genes in ES cells. Nature. 2010;464(7286):306–10.
33. Yoshida K, Miki Y. Role of BRCA1 and BRCA2 as regulators of DNA repair, transcription, and cell cycle in response to DNA damage. Cancer Sci. 2004;95(11):866–71.
34. Roy R, Chun J, Powell SN. BRCA1 and BRCA2: different roles in a common pathway of genome protection. Nat Rev Cancer. 2011;12(1):68–78.
35. Knudsen ES, Pruitt SC, Hershberger PA, Witkiewicz AK, Goodrich DW. Cell cycle and beyond: exploiting new RB1 controlled mechanisms for cancer therapy. Trends Cancer. 2019;5(5):308–24.
36. Kofuji S, Kimura H, Nakanishi H, Nanjo H, Takasuga S, Liu H, et al. INPP4B Is a PtdIns(3,4,5)P3 Phosphatase that can act as a tumor suppressor. Cancer Discov. 2015;5(7):730–9.
37. Hanahan D. Hallmarks of cancer: new dimensions. Cancer Discov. 2022;12(1):31–46.
38. Martinez-Rodriguez OP, Thompson-Bonilla MDR, Jaramillo-Flores ME. Association between obesity and breast cancer: Molecular bases and the effect of flavonoids in signaling pathways. Crit Rev Food Sci Nutr. 2020;60(22):3770–92.
39. Ando S, Catalano S. The multifactorial role of leptin in driving the breast cancer microenvironment. Nat Rev Endocrinol. 2011;8(5):263–75.
40. Robinson DR, Wu YM, Lonigro RJ, Vats P, Cobain E, Everett J, et al. Integrative clinical genomics of metastatic cancer. Nature. 2017;548(7667):297–303.

41. Wang X, Lyu J, Ji A, Zhang Q, Liao G. Jarid2 enhances the progression of bladder cancer through regulating PTEN/AKT signaling. Life Sci. 2019;230:162–68.
42. Adhikari A, Mainali P, Davie JK. JARID2 and the PRC2 complex regulate the cell cycle in skeletal muscle. J Biol Chem. 2019;294(51):19451–64.
43. Nassar D, Blanpain C. Cancer stem cells: basic concepts and therapeutic implications. Annu Rev Pathol. 2016;11:47–76.
44. Atashzar MR, Baharlou R, Karami J, Abdollahi H, Rezaei R, Pourramezan F, et al. Cancer stem cells: A review from origin to therapeutic implications. J Cell Physiol. 2020;235(2):790–803.
45. Chang JC. Cancer stem cells: Role in tumor growth, recurrence, metastasis, and treatment resistance. Medicine (Baltimore). 2016;95(1 Suppl 1):S20–5.
46. Wang Q, Wu J, Wei H, Huang H, Huang Y, Fang H, et al. JARID2 promotes stemness and cisplatin resistance in non-small cell lung cancer via upregulation of Notch1. Int J Biochem Cell Biol. 2021;138:106040.
47. Cheng C, Geng F, Cheng X, Guo D. Lipid metabolism reprogramming and its potential targets in cancer. Cancer Commun (Lond). 2018;38(1):27.
48. Chung SJ, Nagaraju GP, Nagalingam A, Muniraj N, Kuppusamy P, Walker A, et al. ADIPOQ/adiponectin induces cytotoxic autophagy in breast cancer cells through STK11/LKB1-mediated activation of the AMPK-ULK1 axis. Autophagy. 2017;13(8):1386–403.
49. Parida S, Siddharth S, Sharma D. Adiponectin, obesity, and cancer: Clash of the bigwigs in health and disease. Int J Mol Sci. 2019;20(10):2519.
50. Wang T, Fahrmann JF, Lee H, Li YJ, Tripathi SC, Yue C, et al. JAK/STAT3-Regulated fatty acid beta-oxidation is critical for breast cancer stem cell self-renewal and chemoresistance. Cell Metab. 2018;27(1):136–50 e5.
51. Zhang C, Yue C, Herrmann A, Song J, Egelston C, Wang T, et al. STAT3 activation-induced fatty acid oxidation in CD8(+) T effector cells is critical for obesity-promoted breast tumor growth. Cell Metab. 2020;31(1):148–61 e5.

SUPPORTING INFORMATION

Additional supporting information can be found online in the Supporting Information section at the end of this article.

How to cite this article: Liu W, Zeng Y, Hao X, Wang X, Liu J, Gao T, et al. JARID2 coordinates with the NuRD complex to facilitate breast tumorigenesis through response to adipocyte-derived leptin. Cancer Commun. 2023;43:1117–1142.
https://doi.org/10.1002/cac2.12479